Organometallic Science
https://www.sciltp.com/journals/os

Review

N-Heterocyclic Carbenes in Advanced Electrocatalysis: From Molecular Complexes to Hybrid Metal Nanostructures

Amalia Rapakousiou [1,2]

[1] Theoretical and Physical Chemistry Institute, National Hellenic Research Foundation, 48 Vassileos Constantinou Avenue, 11635 Athens, Greece; arapak@eie.gr
[2] Department of Biological Applications and Technology, University of Ioannina, 45110 Ioannina, Greece

How To Cite: Rapakousiou, A. N-Heterocyclic Carbenes in Advanced Electrocatalysis: From Molecular Complexes to Hybrid Metal Nanostructures. *Organometallic Science* **2025**, *1*(1), 2.

Received: 4 August 2025
Revised: 26 August 2025
Accepted: 27 August 2025
Published: 2 September 2025

Abstract: N Heterocyclic carbenes (NHCs) have emerged as powerful and versatile ligands in electrocatalysis, offering a unique combination of strong σ-donor and π-acceptor properties, exceptional thermal and electrochemical stability, and broad structural tunability. This review surveys recent advances in NHC-based electrocatalytic systems across a spectrum of key energy-relevant transformations —including CO_2 reduction (CO_2RR), hydrogen evolution (HER), oxygen evolution (OER), oxygen reduction (ORR), ammonia oxidation, and urea electrosynthesis. From well-defined molecular complexes to nanostructured hybrids and surface-bound architectures, NHC ligands enable fine control over metal–ligand redox interplay, substrate activation, and reaction selectivity. Their covalent anchoring on conductive supports ensures strong metal–support coupling, maximized active-site exposure, and exceptional long-term durability. Mechanistic insights from operando studies and DFT simulations reveal how NHC coordination shapes charge-transfer steps, stabilizes high-valent intermediates, and enhances multielectron reactivity. Particular attention is paid to macrocyclic and redox-active NHC scaffolds, which offer new opportunities for stabilizing reactive intermediates and mediating proton-coupled electron transfer. Together, these findings highlight the broad utility of NHCs as molecular design elements bridging homogeneous and heterogeneous catalysis. We conclude by outlining emerging ligand architectures and materials integration strategies that will be key for advancing scalable, durable, and selective NHC-based electrocatalytic technologies.

Keywords: N-Heterocyclic carbenes (NHCs); electrocatalysis; CO_2 reduction reaction (CO_2RR); Hydrogen evolution reaction (HER); Oxygen evolution reaction (OER); hybrid nanomaterials

1. Introduction

The global shift toward carbon-neutral energy systems demands robust and efficient technologies for electrochemical transformations such as hydrogen evolution (HER), oxygen evolution (OER), and carbon dioxide reduction (CO_2RR) [1]. These processes underpin vital platforms in renewable energy, including water electrolysis, carbon capture and utilization (CCU), and synthetic fuel generation. However, current catalytic systems face persistent challenges: reliance on scarce noble metals, poor selectivity under competing reactions, instability under harsh redox conditions, and insufficient activity under industrially relevant current densities [2,3].

Molecular ligands offer powerful strategies for tuning catalytic behavior by influencing metal–substrate binding, redox properties, and reaction kinetics [4,5]. Traditional ligands such as phosphines and amines have

facilitated many homogeneous catalytic systems but suffer from limited thermal and electrochemical stability, particularly under strongly reducing or oxidizing potentials. In recent years, N-heterocyclic carbenes (NHCs) have emerged as a compelling class of ligands for electrocatalysis, combining robust metal–carbon bonds with strong σ-donor and π-accepting character and synthetic versatility [6,7]. Comparative studies—discussed in detail throughout this review—have shown that NHC-functionalized systems frequently outperform their phosphine- or amine-ligated counterparts in terms of durability, catalytic turnover, and resistance to ligand loss under electrochemical conditions.

NHCs have demonstrated unique advantages across multiple electrocatalytic contexts. Their strong covalent coordination stabilizes metals in both low and high oxidation states, enabling redox reversibility and resistance to degradation even under prolonged electrolysis [8,9]. Additionally, their electronic tunability allows for fine control over catalytic intermediates, while their compatibility with nanostructured surfaces enables the design of hybrid materials that bridge molecular and heterogeneous catalysis [10,11]. Particularly notable are NHC-ligated nanoclusters, nanocrystals, and surface-anchored complexes on conductive supports, which have shown exceptional activity and durability—especially when combined with nanoscale engineering and high surface dispersion [12,13].

This comprehensive review provides a critical overview of all reported NHC-based electrocatalysts to date, encompassing every known example across key electrochemical transformations—including CO_2 reduction, HER, and OER—as well as emerging applications such as ORR, ammonia oxidation, and urea electrosynthesis (Figure 1). We highlight mechanistic insights where available, including redox modulation, reaction-determining steps, and interfacial charge-transfer properties. Special attention is given to systems where nanoarchitecture, support effects, and covalent anchoring converge to create highly active and durable electrocatalysts. Although the field is still in an early stage—particularly beyond CO_2RR—the rapidly growing body of work reveals common design principles that may guide the development of next-generation carbene-ligated electrocatalytic platforms.

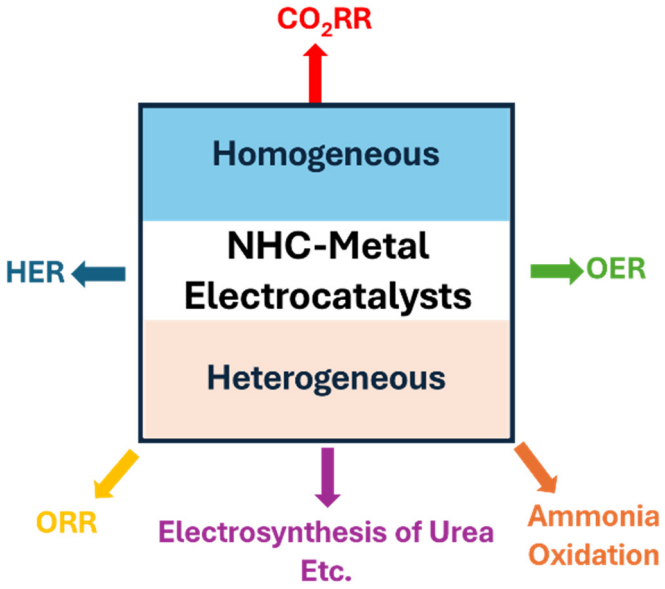

Figure 1. Conceptual framework of NHC–metal electrocatalysts, categorized as homogeneous (top) and heterogeneous (bottom) systems. These architectures enable key electrochemical transformations such as CO_2 reduction (CO_2RR), hydrogen evolution (HER), oxygen evolution (OER), oxygen reduction (ORR), ammonia oxidation, and urea electrosynthesis. The integration of NHC ligands with molecular or nanostructured metal sites supports enhanced stability, selectivity, and redox adaptability.

2. Electrocatalytic CO_2 Reduction with NHC-Based Systems

2.1. Molecular Complexes: Tuning Reactivity through Ligand Design

2.1.1. Nickel

The earliest examples of NHC-Metal electrocatalysts for CO_2 reduction employed well-defined molecular systems, particularly nickel and palladium complexes. In 2011, Chang et al. reported a series of nickel (II)

complexes supported by NHC–pyridine (^{R}bimpy, R = Me, Et, Pr) ligands that demonstrated the ability to reduce CO_2 over H_2O in aqueous media selectively [14]. However, the catalysts exhibited only low turnover frequencies (TOFs = 3.9–5.9 h^{-1}), and prolonged electrolysis at cathodic potentials led to ligand degradation via hydrogenation of conjugated bonds. Catalytic activity emerged at the second reduction wave (−1.69 to −1.46 V vs. SCE), with high selectivity for CO over H_2, although one-electron reduction led to dimerization into inactive Ni(I)–Ni(I) species. Although the overall catalytic activity was limited, this work established that incorporating a strong σ-donor NHC into a mixed NHC/pyridine coordination environment can bias the reaction toward CO_2 activation even in the presence of water. This principle—using NHCs to favor CO_2 reduction over proton reduction—has since guided many subsequent design strategies.

A decade later, Albrecht and co-workers reported Ni(II) complexes with oxo-functionalized mesoionic triazolylidene (C, O-chelating) ligands that reduce CO_2 exclusively to formate with remarkable selectivity (Figure 2a) [15]. In a MeOH/MeCN solvent mixture, these catalysts achieved a Faradaic efficiency (FE) of 83% for formate, the highest reported for any Ni-based CO_2RR system up to then (*Table* 1, entries 1 and 2). Significantly, they maintained this selectivity even with protic additives (including water). Formate selectivity was preserved across a range of proton sources, including water, phenol, and trifluoroethanol (TFE), demonstrating operational robustness under diverse conditions. Catalysis occurred upon reduction at ~−2.31 V vs. Ag/AgCl, while bulk electrolysis was performed at –1.9 V, a relatively high potential that may limit practical efficiency. Catalyst decomposition was observed after extended electrolysis, with NiO and Ni_2O_3 nanoparticles forming on the electrode surface; however, formate selectivity remained high during the active phase, confirming that catalysis originates from the molecular Ni complex. Mechanistic studies (cyclic voltammetry and DFT) implicate a Ni–hydride intermediate as the active species that attacks CO_2, with an observed rate constant K_{obs} up to ~ 370 s^{-1} for CO_2 insertion (Figure 3a)—tuning the electron-donating character of the ligand (e.g., using a 4,6-di-tert-butyl phenolate substituent) strongly influenced activity. The authors also found a striking geometric effect: the *cis* isomers (both NHC donors on the same face) were much more active than the *trans* isomers. The trans-Ni isomer was nearly inactive (k_{obs} ~ 10 s^{-1}), whereas a cis analog reached K_{obs} ≈ 440 s^{-1}. The cis arrangement enforces a distorted square-planar geometry and creates an "internal" proton relay pocket, which likely facilitates the Ni(I)–hydride formation and subsequent CO_2 attack. This study not only set a new benchmark for Ni–NHC catalysis (formate selectivity at >80% FE) but also highlighted how mesoionic NHC frameworks can be tuned both electronically and geometrically to enhance both selectivity and rate.

2.1.2. Palladium

Building on early NHC work with Ni, researchers extended NHC ligation to palladium (Figure 2b) [16]. Wolf et al. described lutidine-linked bis-NHC Pd pincer complexes that electrochemically reduce CO_2 to CO at applied potentials down to −1.75 V (vs. $Ag/AgNO_3$) in the presence of trifluoroacetic acid (Table 1, entry 3). These Pd pincers exhibited a chemically reversible one-electron reduction, forming a long-lived anionic species. DFT calculations showed that the extra electron is delocalized onto the ligand's π system (the lutidine–bis-NHC scaffold) rather than residing on Pd. In effect, the ligand serves as a redox-active reservoir, shifting electron density away from the metal center and suppressing catalyst decomposition pathways that plagued earlier triphosphine-based Pd catalysts. Controlled electrolysis revealed Faradaic efficiencies of 8–9% at −1.75 V and up to 28% at −2.30 V, with significant improvement (up to 47% FE at −2.30 V) upon K^+ addition. The enhanced stability allowed the Pd–bisNHC complexes to turnover CO_2 to CO in the presence of protons, whereas comparable Pd(P^3) systems tended to deactivate.

Structural evolution of the ligand scaffold continued by the same team with the introduction of polyaromatic (phenanthro- and pyrene-annulated) bis-NHCs, which added additional redox capacity to the ligand backbone [17]. As a result, the electron-rich polyaromatic NHC–Pd pincers showed faster initial CO_2-to-CO turnover (Table 1, entry 4). However, the highly delocalized reduction also led to new deactivation modes: during extended electrolysis, these complexes tended to form ligand-centered radical species that dimerized or precipitated as inactive films. In other words, increasing the ligand's electron reservoir boosted activity but at the cost of stability—a tradeoff between electronic richness and operational robustness. Computational analysis of the reduced states supported this interpretation, showing that the polyaromatic pincer's first reduction was ligand-based mainly and that the binding strength of CO (and thus resistance to dissociation) was inversely related to the extent of ligand-centered reduction (related to anion dissociation energies in the pincer scaffold). These Pd studies underscored how redox-active NHC pincers can enhance catalyst durability (by avoiding metal-centered high-spin states) but also cautioned that overly delocalized systems may introduce instability under long-term electrolysis.

2.1.3. Manganese

Transitioning beyond Pd and Ni, manganese (Mn) has emerged as an attractive earth-abundant center for CO_2 reduction. The first Mn electrocatalysts featuring NHC ligands were reported by Agarwal et al. in 2014 (Figure 2c) [18]. They synthesized Mn(I) tricarbonyl complexes with bidentate NHC–pyridyl ligands—specifically, N-methyl-N′-2-pyridylbenzimidazolylidene and N-methyl-N′-2-pyridylimidazolylidene—and showed these could catalyze two-electron CO_2 reduction to CO. Notably, the Mn–NHC complexes displayed a single, concerted two-electron wave in cyclic voltammetry: both the first and second reductions occurred at essentially the same potential. This behavior contrasts with the classic Mn(bipyridine)$(CO)_3$Br system, which undergoes two one-electron reductions separated by ~500–600 mV. The authors attributed this "compressed" redox profile to the strong σ-donor power of the NHC, which raises the Mn(II/I) potential and lowers the Mn(I/0) potential such that they overlap. As a result, the Mn–NHC enters the active Mn^0 state more readily (in one concerted step) without passing through a long-lived Mn^- species. Notably, the Mn–NHC catalyst achieved similar onset potentials and catalytic currents to the bipyridine analogue, meaning the NHC ligand preserved catalytic efficiency while fundamentally altering the electron transfer mechanism. Controlled-potential electrolysis of the imidazolylidene complex under CO_2 yielded a steady Faradaic efficiency of ~34.6% for CO over 4 h, with no H_2 detected by GC, indicating selective CO_2-to-CO conversion over HER (Table 1, entry 5). Additionally, TOF values were 0.08 s^{-1} for the benzimidazolylidene complex and 0.07 s^{-1} for the imidazolylidene complex, compared to 0.14 s^{-1} for Mn–bpy. These findings confirm that the strong-field NHC ligands do not compromise activity, while opening new opportunities for mechanistic tuning and stabilization of reduced intermediates.

This seminal result opened the door to tuning Mn catalysts via NHC ligands to improve kinetics and stability [19]. Indeed, recent work has capitalized on NHC ligation to push Mn catalysts to unprecedented activities. In 2018, Lloret-Fillol and co-workers reported a bis-NHC pincer Mn(I) complex, fac-[Mn$(CO)_3$(bis-MeNHC)Br], which showed exceptional activity for CO_2-to-CO electrocatalysis (Figure 2d) [20]. In anhydrous CH_3CN, it achieved 98% CO selectivity with turnover frequencies (TOF) up to ~2100 s^{-1} (by CV foot-of-wave analysis), already far exceeding bipyridine-based Mn catalysts (Table 1, entry 6). Remarkably, adding a small amount of water (0.56 M) accelerated the catalysis by two orders of magnitude, reaching a TOF_{max} of ~3.2×10^5 s^{-1}—the highest ever reported for a Mn catalyst. This dramatic rate enhancement with water suggests a beneficial proton-coupled electron transfer (PCET) pathway or a faster regeneration of the active Mn–hydride in the presence of protons. The superior performance was attributed to the increased nucleophilicity of the Mn center conferred by the strongly donating bis-NHC ligand (which promotes rapid CO_2 binding and activation), as well as the rigid pincer scaffold that disfavors catalyst dimerization (Figure 3b). Shortly thereafter, a study by Gonell and co-workers systematically examined a series of Mn bis-NHC complexes with different ligand backbones (Figure 2e) [21]. They compared methylene-, ethylene-, and ortho-phenylene-bridged bis(NHC) ligands—denoted as CH_2-, C_2H_4-, and Ph-bis-mim, respectively—where bis-mim refers to bis(N-methylimidazolylidene). These ligands form five-, six-, and seven-membered metallacycles with the Mn center. All complexes displayed high selectivity for CO, with negligible formation of formate or H_2, and maintained strong catalytic activity across the series, although the overpotentials varied notably. (Figure 3c; Table 1, entries 7–9). Crucially, the most rigid seven-membered (Ph-bis-mim) complex retained similarly fast kinetics while lowering the overpotential by 120–190 mV compared to the six-membered analog. Although the exact mechanistic pathway was not fully resolved, fast-scan cyclic voltammetry revealed that the rate-determining step is chemical in nature rather than electron transfer, consistent with a CO_2 binding or activation event. The catalytically active species is likely the halide-free Mn(I)$(CO)_4$ complex, as both Mn–Br and Mn–CO^+ analogues exhibited comparable rate constants. The authors proposed that the rigid ortho-phenylene bridge induces axial asymmetry and favourable orbital alignment between Mn, CO, and NHC ligands, potentially stabilizing key intermediates and lowering the overpotential. These features support a general mechanism involving Mn–CO_2 adduct formation, followed by protonation and CO release.

These findings reinforce that backbone rigidity and asymmetry in bis-mim ligands can be strategically tuned to lower overpotentials and preserve fast kinetics, paving the way for future catalyst optimization via secondary coordination effects. Together, these Mn studies firmly establish that bis-NHC ligands can dramatically enhance first-row catalytic performance, and that fine-tuning the NHC linker (flexibility, ring size) provides a handle to optimize overpotential, turnover frequency, and catalyst longevity.

2.1.4. Iron

While Mn has flourished, iron—another earth-abundant 3d metal—has also seen significant advances with NHC ligands. One strategy has been to combine NHC donors with redox-active polypyridines to modulate Fe's properties. For example, Miller, Lloret-Fillol and Gonell designed Fe(II) catalysts featuring a terpyridine (tpy)

ligand and a chelating bis-carbene (Figure 2f) [22]. In one complex, $[Fe(tpy)(C–NHC–C)(MeCN)]^{2+}$, the Fe center is coordinated by a tridentate terpyridine and a bidentate methylene-bridged bis(N-methylimidazolylidene), with one MeCN completing the octahedral coordination. This system was shown to efficiently convert CO_2 to CO at a very low overpotential (onset $\eta \approx 0.2$ V) while maintaining fast kinetics (observed rate constant k_{obs} ~34 s^{-1})—a combination that is difficult to achieve (Table 1, entry 10). By comparing variants of the NHC ligand, the authors demonstrated that increasing the carbene's donor strength accelerates the turnover rate *without* negatively shifting the catalyst's reduction potentials. In other words, they could boost the catalytic rate independently of the thermodynamic driving force, effectively decoupling kinetics from overpotential. This behavior contrasts with a previously studied Fe–NHC–pyridyl system, in which pyridine hemilability was essential for CO release. In the bis-mim case, irreversible NHC dissociation occurs only after extended catalysis, and the rate-limiting step is instead CO_2 binding—highlighting how different NHC architectures shift the mechanistic bottleneck while retaining low η. Detailed mechanistic studies (including foot-of-wave analysis and digital simulations) indicated that the rate-determining step is nucleophilic attack of a reduced Fe-carbonate or Fe–hydride species on CO_2 (Figure 3d). Strengthening the NHC donor favored this step (by increasing electron density at Fe), yet, because the terpyridine was redox-non-innocent and bore the brunt of redox changes, the overall Fe^{II}/Fe^{I} couple remained at a low potential. This illustrates a modular strategy for catalyst design: pairing a redox-active electron buffer ligand (tpy) with a potent trans-effect NHC ligand allows one to tune the kinetics (through the NHC's influence on intermediate barriers). In contrast, the redox-active ligand maintains a favorable potential window.

A complementary Fe system reported around the same time underscored the importance of ligand dynamics. In that work, an Fe(II) complex with a pyridyl-NHC ligand and a terpyridine was shown to achieve >95% FE for CO with an overpotential of only ~150 mV under CO_2 flow conditions (Figure 2g; Table 1, entry 11) [23]. A key insight was that the pyridyl-NHC ligand is hemilabile—it can dissociate and reassociate—enabling the Fe center to switch coordination geometry during the catalytic cycle (Figure 3e). DFT and experimental data suggested that after CO_2 binds and is reduced to CO, the pyridyl-NHC transiently dissociates (or reconfigures) to allow CO release from the Fe center, then re-coordinates to continue the cycle. This kind of reversible coordination (facilitated by the strong trans influence of the NHC, weakening the Fe-pyridine bond) is especially beneficial for Fe, which has a higher propensity for ligand lability than its heavier congeners Ru or Os. The result is a catalyst that turnover faster at low driving force because it avoids product inhibition (CO binding) via dynamic ligand behavior. These studies on Fe–NHC–polypyridine hybrids highlight how combining redox-active backbones and hemilabile NHC donors can yield first-row catalysts with both low overpotential and high turnover frequency. The concept is analogous to enzyme active sites: a flexible first coordination sphere and a redox-tunable cofactor can circumvent the usual trade-off between rate and driving force.

Computational modeling of such Fe and Co systems [24] reinforces these ideas, showing that factors like planarity vs. non-planarity of NHC chelates, ligand donor strength, and hemilability profoundly affect CO_2 binding modes and proton-coupled electron transfer steps. Moreover, theory suggests that expanding the design strategy to secondary and outer-sphere interactions (e.g., incorporating proton relays or second-sphere hydrogen-bonding)—again echoing enzymatic principles—could further enhance performance. In summary, the Fe and Co examples illustrate a powerful lesson: by tuning the primary coordination sphere (through NHC and polypyridine ligands), one can independently optimize catalytic rate and catalytic efficiency, something that is difficult to achieve with rigid, redox-innocent ligand frameworks.

A novel approach by Meyer, Siewert, and co-workers employed NHC macrocycles as ligand scaffolds on iron, creating analogues of porphyrins where all four donor atoms are carbene carbons. (Figure 2h) [25]. They reported the first such complex, a 16-membered tetracarbene macrocycle coordinated to Fe(II) as an equatorial NHC plane. This complex $[LFe(MeCN)_2]^{2+}$ (with L = C_4 ligand) can be viewed as an "organometallic heme"—it has a similar planar structure to Fe-porphyrin, but the NHC donors are much stronger σ-donors and are redox-inactive. Consequently, the Fe center in $[LFe(MeCN)_2]^{2+}$ exhibits very different electrochemical behavior from a heme: the Fe(II)/Fe(I) and Fe(I)/Fe(0) reductions are significantly shifted and are metal-centered (the ligand framework remains unoxidized). Under CO_2, this tetracarbene–Fe catalyst showed >90% FE for CO and an exceptionally high initial turnover frequency (Table 1, entries 12 and 13). The foot-of-wave analysis indicated a $k_{obs} \approx 7.8 \times 10^3$ s^{-1} immediately after activation, which is orders of magnitude above typical molecular Fe catalysts. Even over longer electrolysis, it sustained fast catalysis with negligible degradation. The authors found that if one axial MeCN ligand is replaced by CO (giving $[LFe(CO)(MeCN)]^{2+}$ in situ), the catalyst's stability improves (higher tolerance to prolonged electrolysis) while the rate remains very high (k_{obs} ~3.1×10^3 s^{-1}, only slightly lower than the MeCN/MeCN form). Spectroelectrochemical IR experiments revealed a mechanism involving CO_2 disproportionation: two CO_2 molecules are reduced in tandem—one to CO, and one to CO_3^{2-} (carbonate). Specifically, the reduced Fe^0 species $[LFe^0(CO)]$ (with an open axial site and an electron in the formerly dz^2 orbital)

can bind CO_2 and facilitate its bending and reduction to CO (as a bound CO ligand), while a second CO_2 reacts with an oxygen atom (O_2^- transfer) to form CO_3^{2-} (Figure 3f). This mechanism is reminiscent of what is seen in some heterogeneous processes and in enzyme systems like carbon monoxide dehydrogenase, and it showcases the ability of a strong NHC ligand field to generate a highly reducing, yet coordinatively unsaturated, Fe^0 center that can activate CO_2 in unconventional ways. The broader implication is that NHC macrocycles offer a robust, tunable platform for first-row metals. Unlike porphyrins, which delocalize electrons extensively on the ligand, NHC macrocycles tend to keep electrons on the metal (enabling authentic Fe(0) chemistry). They also resist oxidative degradation (strong C–Fe bonds and no dangling protonatable heteroatoms), which likely contributes to the exceptional stability observed. This new class of Fe catalysts extends the scope of NHCs from "supporting" ligands to primary framework ligands, and early results suggest they can rival or surpass the activity of traditional porphyrin systems while offering new mechanistic pathways (e.g., the CO_2 disproportionation noted above).

2.1.5. Cobalt

Cobalt, another earth-abundant metal, has benefited from NHC ligand designs as well. Jurss and co-workers introduced bipyridyl-NHC macrocyclic ligands for Co(II/III), achieving remarkable performance in CO_2 electroreduction under both organic and truly aqueous conditions (Figure 2i–k) [26]. In these complexes, a bipyridine unit is incorporated into a macrocycle with NHC donors, creating an extended conjugated ligand that can share electrons with the metal. A series of Co complexes (dubbed 1-Co, 2-Co, 3-Co with increasing macrocycle rigidity) was evaluated. Mechanistic rate studies showed a first-order dependence on [Co] and [CO_2], and second-order in [H_2O], consistent with a two-proton, two-electron reduction to CO (i.e., a rate law indicating two protons from water are involved in the rate-limiting steps). The catalysts displayed exceptional CO selectivity: for example, in acetonitrile with just 2% water added, the most rigid macrocycle (3-Co) gave ~98% FE for CO. Even in pure aqueous bicarbonate buffer (pH ~7), it maintained ~93% FE for CO, a level of selectivity and activity rarely seen with molecular catalysts in water. A significant trend was that increasing the macrocycle's rigidity and planarity (from 1-Co to 3-Co) improved performance (Table 1, entries 14–16). The most flexible ligand (1-Co, which is not macrocyclic) showed lower turnover numbers and some deactivation, whereas the fully cyclic, rigid ligand in 3-Co not only enhanced activity but also prevented catalyst degradation (no dissociation or decomposition observed over prolonged electrolysis). DFT calculations provided insight into the electronic effects at play. For the loosely-linked ligand, the first reduction was largely ligand-centered (forming a bipyridine radical anion). In contrast, for the rigid macrocycle, the reduction had more metal character—resulting in a more nucleophilic Co(I) center that binds CO_2 more strongly. Essentially, the bipyridyl–NHC macrocycle acts as a tunable redox-active ligand, and when its geometry is constrained, it pushes more electron density onto the metal during reduction. That, in turn, facilitates CO_2 coordination and subsequent electron/proton transfer. Another advantage of these NHC-containing macrocycles is their inherent water solubility (especially compared to traditional porphyrins or phthalocyanines, which are often insoluble). This, combined with the low overpotential (~0.42 V) and high stability, makes them promising candidates for practical CO generation in electrolyzers. In summary, the Co–NHC macrocyclic systems showcase how integrating NHC units into a *conjugated macrocyclic ligand* can marry the benefits of secondary coordination effects (e.g., ligand non-innocence and rigidity) with the donor strength of NHCs, yielding catalysts that operate efficiently in water—a critical step toward real-world CO_2 reduction applications.

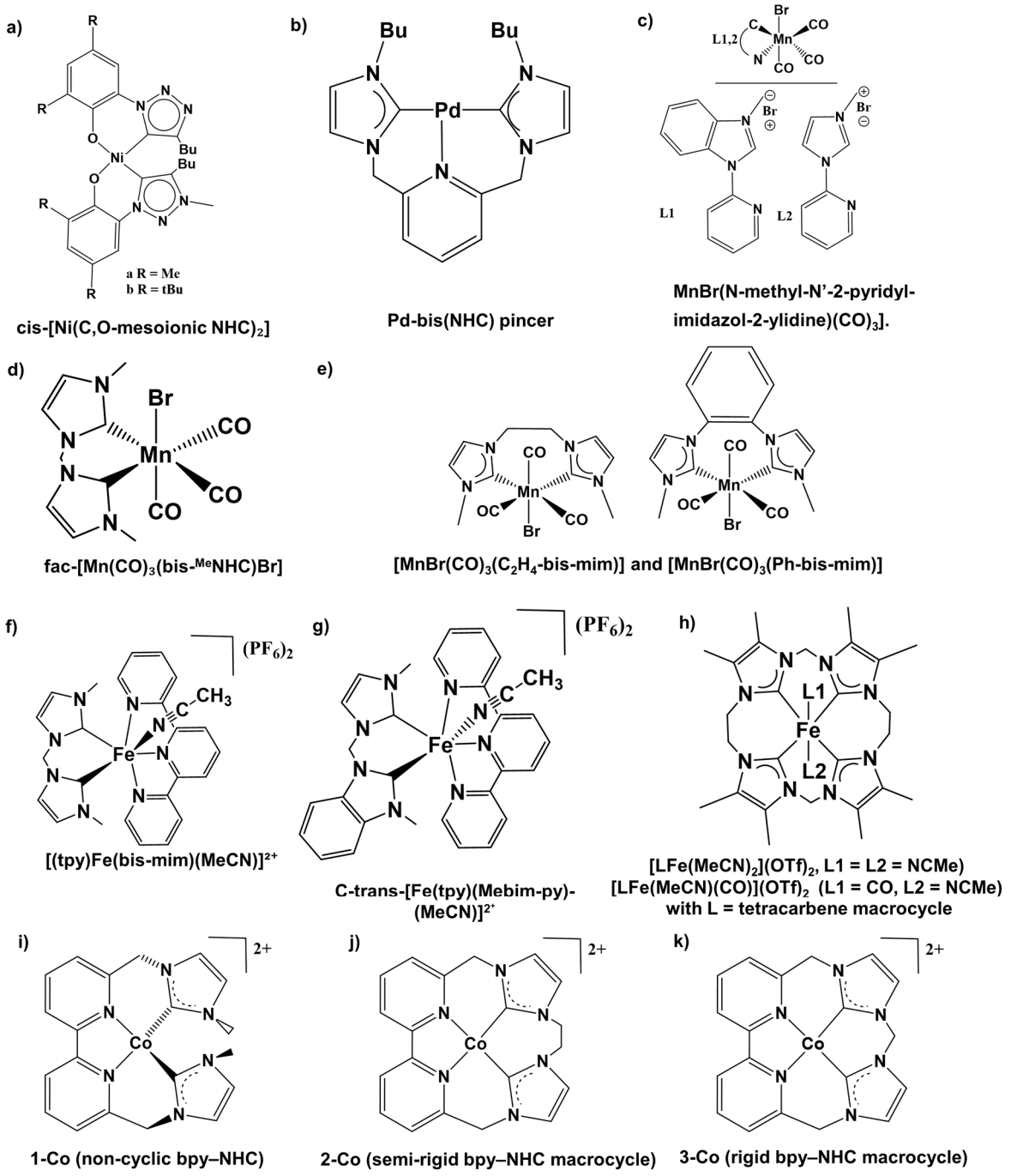

Figure 2. Molecular structures of NHC-metal electrocatalysts. Structures redrawn from: (**a**) Ref. [15], (**b**) Ref. [16], (**c**) Ref. [18], (**d**) Ref. [20], (**e**) Ref. [21], (**f**) Ref. [22], (**g**) Ref. [23], (**h**) Ref. [25], (**i**,**j**,**k**) Ref. [26].

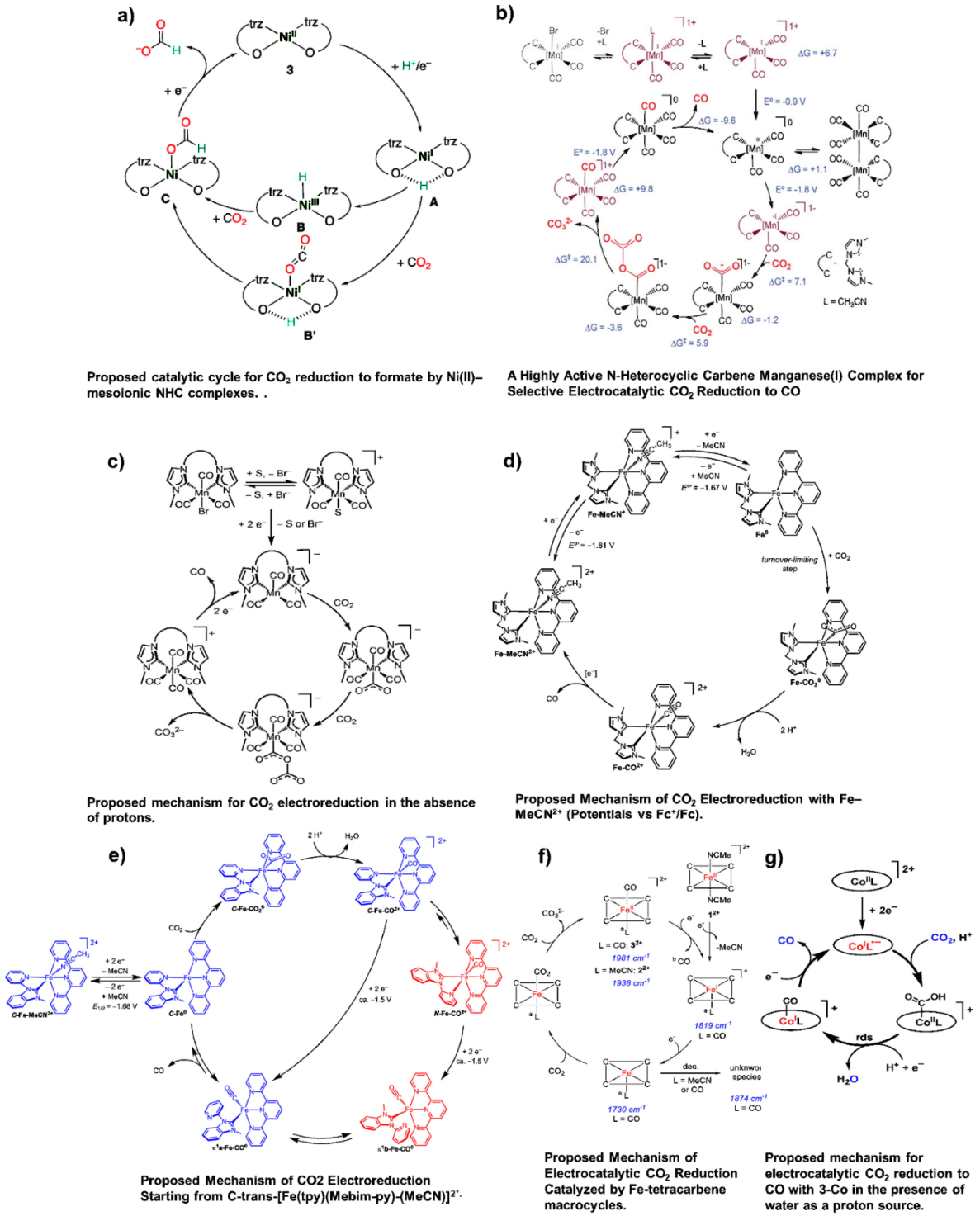

Figure 3. Proposed electrocatalytic mechanisms for NHC-Metal complexes. Reproduced from: (**a**) Ref. [15] with permission from the Royal Society of Chemistry, (**b**,**c**) Ref. [20,21] with permission from the Wiley-VCH GmbH, (**d**–**g**) Refs. [22,23,25,26] with permission from the American Chemical Society.

Table 1. NHC-based molecular electrocatalysts for CO_2RR.

Entry	Molecular Electrocatalyst	Metal	Conditions	CPE Potentials vs. RHE *	Product	FE (%)	Ref.
1	**cis-[Ni(C,O-mesoionic NHC)$_2$], R = tBu**	Ni (II)	MeOH/MeCN (1:50), 0.1 M NBu_4PF_6, glassy carbon	−1.70	Formate	83	[15]
2	**cis-[Ni(C,O-mesoionic NHC)$_2$], R = Me**	Ni (II)	MeOH/MeCN (1:50), 0.1 M NBu_4PF_6, glassy carbon	−1.70	Formate	74	[15]
3	**Pd-bis(NHC) pincer**	Pd (II)	DMF, 0.1 M $TBAPF_6$, 10 mM TFA, +50 mM K^+, RVC	−2.01 V	CO	47	[16]
4	**Pd-bis(NHC) pincer (phenanthrol-annulated)/ pyreno-annulated)**	Pd (II)	DMF, 0.1 M [n-Bu_4N]PF_6, glassy carbon	~−1.4 V	CO	27/12	[17]
5	**MnBr(N-methyl-N'-2-pyridylimidazol-2-ylidine)(CO)$_3$].**	Mn (I)	CH_3CN (5% H_2O), 0.1 M TBAP, glassy carbon	−1.22 V	CO	34.6	[18]
6	**fac-[Mn(CO)$_3$(bis-^{Me}NHC)Br],**	Mn (I)	CH_3CN, 0.1 M $TBAPF_6$, 0.22 M H_2O, glassy carbon	−1.68 V	CO	98	[20]
7	**CH_2-bis-mim**	Mn (I)	CH_3CN, 0.1 M $TBAPF_6$, glassy carbon/+1% H_2O	−0.71 V/ −0.51 V	CO	92/ 98	[21]
8	**C_2H_4-bis-mim**	Mn (I)	CH_3CN, 0.1 M $TBAPF_6$, glassy carbon/+1% H_2O	−0.56 V/ −0.32 V	CO	100/ 99	[21]
9	**Ph-bis-mim**	Mn (I)	CH_3CN, 0.1 M $TBAPF_6$, glassy carbon/+1% H_2O	−0.59 V/ −0.33 V	CO	93/ 92	[21]
10	**[(tpy)Fe(bis-mim)(MeCN)]$^{2+}$**	Fe (II)	CH_3CN, 0.1 M $TBAPF_6$, +5% H_2O, glassy carbon	−1.11 V	CO	72/90 (at CO_2 constant flow)	[22]
11	**C-trans-[Fe(tpy)(Mebim-py)-(MeCN)]$^{2+}$**	Fe (II)	CH_3CN, 0.1 M $TBAPF_6$, +5% H_2O, glassy carbon	−1.04 V	CO	33 ± 5%	[23]
12	**[LFe(MeCN)$_2$](OTf)$_2$ (L = tetracarbene macrocycle)**	Fe (II)	CH_3CN, 0.1 M $TBAPF_6$, +5% H_2O, glassy carbon	−1.57 V	CO	92 ± 5%	[25]
13	**[LFe(MeCN)(CO)](OTf)$_2$ (L = tetracarbene macrocycle)**	Fe (II)	CH_3CN, 0.1 M TBAPF6, +5% H_2O, glassy carbon	−1.57 V	CO	120 ± 13%	[25]
14	**1-Co (non-cyclic bpy–NHC)**	Co (II)	H_2O, 0.1 M $NaClO_4$, mercury	−0.69 V	CO	87	[26]
15	**2-Co (semi-rigid bpy-NHC macrocycle)**	Co (II)	H_2O, 0.1 M $NaClO_4$, mercury	−0.62 V	CO	94	[26]
16	**3-Co (rigid bpy–NHC macrocycle)**	Co (II)	H_2O, 0.1 M $NaClO_4$, mercury/H_2O, 0.1 M $NaHCO_3$, mercury	−0.64 V/ −0.51 V	CO	97/ 93	[26]
17	**[RuII(tpy)(Mebim-py)(H2O)](PF6)2 (Mebim-py ¼ 3-methyl-1-pyridyl-benzimidazol-2-ylidene)**	Ru (II)	H_2O, 0.5M $NaHCO_3$, carbon cloth	−0.70 V/−1.00 V	H_2/CO (syngas) (0.5:1)/ (2.6:1)	99% (combined)	[27]
18	**[Ru(tpy)(Mebim-py)($NCCH_3$)]$^{2+}$ (C-trans)**	Ru (II)	CH_3CN, 0.1 M TBAPF6, glassy carbon	−1.51 V	CO	87%	[28]

* All CPE potentials have been converted to the RHE scale for comparison. Original reference electrodes are preserved in-text as reported in the primary literature. Conversions used standard offsets (e.g., Fc^+/Fc + 0.64 V, Ag/AgCl + 0.197 V, SCE + 0.241 V), with pH approximated from experimental conditions.

2.1.6. Ruthenium

Ruthenium-based NHC complexes have shown unique potential for tandem electrochemical transformations, combining CO_2 reduction and water oxidation in a single system. A compelling example is the Ru(II) complex $[Ru(tpy)(Mebim\text{-}py)(H_2O)]^{2+}$, where *tpy* is 2,2′:6′,2″-terpyridine and *Mebim-py* is a pyridyl-substituted benzimidazolylidene ligand [27]. Meyer and co-workers demonstrated that this single-site complex catalyzes the co-electroreduction of CO_2 and H_2O in aqueous $NaHCO_3$ to generate tunable syngas mixtures ($CO + H_2$) under mild conditions.

By adjusting the cathodic potential and solution pH, the H_2/CO product ratio can be varied from ~0.5:1 up to 4:1. At an applied potential of −1.2 V vs. NHE, the system reaches up to 66% CO content in the gas mixture, with a combined Faradaic efficiency of ~99% (Table 1, entry 17). At more negative potentials, H_2 evolution dominates, but CO formation remains significant. Mechanistic investigations revealed that both CO and H_2 evolution proceed via a common two-electron reduced intermediate, $[Ru(tpy^{-})(Mebim\text{-}py^{-})(S)]^0$, where *S* is a labile solvent or water ligand. The competition between CO_2 binding and hydride formation at this intermediate governs product selectivity. Significantly, this Ru–NHC catalyst also operates as a water oxidation catalyst at the anode, enabling full-cell electrolysis of CO_2/H_2O into syngas (cathode) and O_2 (anode) with an overall energy efficiency of ~50%. This dual reactivity in water highlights the role of NHC ligands in stabilizing redox-active intermediates and modulating catalytic pathways under challenging aqueous conditions.

Further mechanistic insight into Ru–NHC systems was provided by Gonell et al., who explored the role of the trans effect in asymmetric Ru(II) terpyridine–carbene complexes (Figure 3g) [28]. They synthesized both N-trans and C-trans isomers of $[Ru(tpy)(Mebim\text{-}py)(NCCH_3)]^{2+}$, along with their corresponding CO adducts, to examine the effect of NHC position on CO_2 reduction performance. Electrochemical experiments in dry MeCN (0.1 M $TBAPF_6$) revealed that the N-trans precursor undergoes reduction-induced isomerization to the more active C-trans geometry, placing the strong NHC donor trans to the CO_2 binding site. This positioning weakens the Ru–CO bond and facilitates fast product release. The C-trans isomer exhibited an observed rate constant (k_{obs}) of ~2400 s^{-1} at −1.73 V vs. Fc^+/Fc, with Faradaic efficiencies >95% for CO (Table 1, entry 18). In contrast, the N-trans isomer showed much slower kinetics and inefficient CO release. This study elegantly shows how rational ligand placement, guided by the NHC's trans effect, and pairing with a redox-active tpy backbone, enables kinetic acceleration without raising overpotential—a powerful strategy for designing efficient CO_2 electrocatalysts.

2.1.7. Rhenium

Rhenium, although not earth-abundant, has long been a benchmark metal for CO_2 reduction studies. NHC ligands have been used to modify the classic $Re(bipyridine)(CO)_3Cl$ platform, even if they did not show any particular promise [29]. A fascinating mechanistic insight regarding this was provided, though, by Luca and co-workers in 2020, who directly compared analogous Mn and Re pincer complexes with bis-NHC ligands [30]. They examined Mn(I) and Re(I) tricarbonyl complexes bearing a pyridine-2,6-bis(NHC) pincer (denoted $M(CO)_3(CNC)BnX$, where CNC is the bis-NHC pincer and BnX is a benzyl halide axial ligand). Strikingly, under identical conditions, the Mn pincer was an extraordinarily active CO_2-to-CO catalyst, while the Re pincer showed no catalytic turnover. Using EPR spectroscopy and DFT, the authors discovered that the key one-electron-reduced intermediates had very different electronic structures. The Mn complex forms a *metalloradical* Mn^0 species with about 66% of the unpaired electron density localized on the Mn center. This high degree of metal-centered spin (with the remaining 34% delocalized on the ligand) corresponds to a nucleophilic "Mn•" radical that readily binds and activates CO_2. In contrast, the reduced Re analog has only ~38% of the spin on Re, with the majority of the electron density delocalized over the bis-NHC ligand framework. In effect, the Re^0 state is a ligand-centered radical—the Re atom is more like a closed-shell Re(I) with a radical anion ligand. Consequently, the Re–CO_2 adduct formation is hindered (the Re center is less nucleophilic and the Re–CO bond is weaker due to significant ligand involvement in the reduction). The DFT calculations showed that this difference imposes a larger kinetic barrier for CO_2 insertion in the Re system, rendering it catalytically inactive. In contrast, the Mn system has a low barrier and proceeds readily. This comparison is illuminating: it shows that for effective CO_2 reduction, a proper balance of metal- vs. ligand-centered reduction is critical. Too much electron delocalization (as in the Re case) can undermine the key metal–CO_2 binding interaction, while a metal-centered radical (as in Mn) is highly reactive toward CO_2. This is an important design principle for redox-active pincer ligands. While they can impart stability and multi-electron capacity, one must ensure the reduced state still retains sufficient "metalloradical" character to engage CO_2. The lesson applies broadly to NHC-based systems: the degree and locus of spin density in reduced intermediates can dictate catalytic outcomes, and careful tuning of ligand electronics can switch a system from inactive to highly active. This mechanistic insight adds a new dimension to catalyst design—emphasizing not just

static properties like donor strength or redox potentials, but also the dynamic electronic configuration of transient species in the catalytic cycle [31].

2.1.8. Concluding Remarks for NHC-Based Molecular Electrocatalysts for CO_2RR

Taken together, the studies above survey the landscape of molecular NHC–metal electrocatalysts for CO_2 reduction. They illustrate several key design strategies enabled by N-heterocyclic carbenes:

(1) Strong σ-donation and modular electronics: NHCs significantly enhance metal electron density, which promotes CO_2 activation and facilitates multi-electron pathways (e.g., formate formation with Ni, rapid CO evolution with Mn). Their modular nature—via backbone substitution, mesoionic tuning, or ring fusion—allows fine-tuning of both electronic and steric environments to balance activity and overpotential. Mechanistic studies, such as those comparing Mn and Re pincer complexes, highlight the importance of redox localization: while the Mn bis-NHC system exhibits a Mn^0 metalloradical intermediate with 66% spin density on the metal, the inactive Re analog localizes the added electron on the ligand, suppressing catalysis.

(2) Mixed-donor and redox-active ligand environments: Combining NHCs with donors such as pyridines or terpyridines creates hybrid ligand frameworks that stabilize reduced states while preserving metal-centered reactivity. These systems, including Pd, Fe, and Co complexes, leverage ligand-based charge storage to achieve low overpotentials. However, excess delocalization onto the ligand—as seen in specific Re and Ru complexes—can limit substrate binding. Conversely, Fe tetracarbene and terpyridine–NHC complexes exhibit charge localization on Fe^0 centers that efficiently bind and convert CO_2 to CO upon protonation.

(3) Geometric control and secondary-sphere effects: Rigid NHC frameworks enforce favorable metal–ligand geometries (e.g., cis orientation in Ni–C, O chelates, macrocyclic preorganization in Co–NHC complexes), facilitating CO_2 binding, proton delivery, and product release. Pendant amines or hemilabile donors in NHC-containing scaffolds act as internal proton relays, enabling rapid turnover at mild potentials. These features mirror enzyme-like strategies across the first, second, and third coordination spheres and are particularly well accommodated by the tunable periphery of NHC ligands.

(4) Stability and durability under electrocatalytic conditions: A unifying strength of NHC ligands is their exceptional robustness under electrochemical stress. Their strong M–C(NHC) bonds and resistance to hydrolysis or oxidative degradation allow them to outperform traditional phosphine or amine-based ligands in long-term CO_2RR. Examples include the cyclam–Ni vs. triazolylidene–Ni comparison, where the latter shows significantly greater longevity, and the Mn–CNC vs. Mn–tpy system, in which the NHC pincer maintains activity over many cycles while the tpy complex decomposes rapidly.

Looking ahead, these principles position NHC ligands as versatile tools in the development of next-generation CO_2RR catalysts. Future efforts may focus on translating these design elements to earth-abundant metals, achieving selective multi-carbon product formation, or enabling tandem catalytic cycles. Their ability to combine stability, tunability, and mechanistic clarity makes NHCs uniquely suited to address these emerging challenges in molecular electrocatalysis. Indeed, some of the most selective and long-lived molecular CO_2RR catalysts to date—across different metals—feature NHC donors (e.g., the Ni formate system, the Co macrocycle, the Fe tetracarbene) [32].

However, despite the precision and mechanistic insight afforded by molecular platforms, they often face limitations in long-term stability, conductivity, and scalability. To overcome these challenges and bring molecular-level control closer to practical implementation, a new generation of hybrid systems has emerged. These approaches seek to integrate NHC ligands directly into metal surfaces, nanoparticles, or conductive supports—creating interfaces that retain the tunability of molecular design while benefiting from the robustness of heterogeneous materials.

2.2. Hybrid Systems: NHC-ligands at the Molecular–Metal Material Interface

Building on the molecular design principles above, recent efforts have explored how NHC ligands can interface with nanostructured metal surfaces to create hybrid electrocatalysts with enhanced performance. These systems retain the tunability of molecular ligands while benefiting from the conductivity and robustness of metallic supports.

2.2.1. Gold and Palladium

For example, in 2016 Chang and co-workers reported an NHC-functionalized gold nanoparticle (AuNP) catalyst which exhibit a Faradaic efficiency (FE) of 83% for CO_2-to-CO conversion (vs. 53% for the parent AuNP) in a CO_2-saturated $KHCO_3$ buffer at −0.57 V, exhibiting a 7.6-fold higher current density (normalized to the electrochemically active Au surface area) (Figure 4a) [33]. Control experiments using free NHC ligands or a

molecular Au–NHC complex showed minimal catalytic response, confirming that the observed activity is intrinsic to the surface-bound carbene–Au hybrid. Tafel analysis showed the NHC-modified Au had a much lower slope (72 mV/dec) than the unmodified Au (138 mV/dec), indicating a change in rate-determining step and that the carbene–Au bond altered the reaction mechanism. The parent Au NPs exhibited a Tafel slope consistent with a rate-limiting single-electron transfer to CO_2. In contrast, the NHC-functionalized Au favored a faster pre-equilibrium electron transfer followed by a rate-limiting chemical step. This study by Chang, Yang and co-workers was one of the first to demonstrate that surface-bound NHCs could serve as more than just stabilizers—they could actively modulate reactivity and selectivity [34]. Mechanistically, the authors attributed the enhanced performance to strong σ-donation from the NHC, which renders the Au surface more electron-rich and thereby facilitates CO_2 activation. Additionally, NHC coordination was proposed to restructure the Au surface, increasing defect sites favorable for catalysis. Notably, spectroscopic characterization (FT-IR, solid-state ^{13}C NMR, Pb underpotential deposition) confirmed the chemical and electrochemical stability of the NHC layer before and after catalysis. Importantly, ligand sterics were found to modulate activity, as bulkier NHCs gave lower FE(CO), highlighting a structure–activity correlation reminiscent of homogeneous catalysis.

The same group applied a similar approach to palladium: a chelating tris-NHC ligand was grafted onto a Pd foil, yielding a hybrid electrode with dramatically improved CO_2RR activity (Figure 4b). The tris-NHC–Pd shifted the CO_2RR onset by ~+0.27 V (from −0.385 V to −0.12 V vs. RHE) and showed a 32-fold increase in formate production rate (C1 products) with high FE (86% with 82% formate and 4% CO vs. 23% on bare Pd with CO as the main product) [35]. The NHC-functionalized Pd showed a much lower Tafel slope (85 mV/dec vs. 157 mV/dec for bare Pd), consistent with a pre-equilibrium electron transfer and a chemical rate-limiting step. It also exhibited sustained activity compared to a monodentate NHC on Pd. This enhancement was attributed to the chelate effect—by binding the metal surface at multiple points, the tris-NHC both boosts reactivity and prevents deactivation. Indeed, the chelating NHC ligand stabilized surface sites and maintained catalytic activity over time, underscoring how *multidentate* ligand architecture can be as valuable on surfaces as it is in homogeneous catalysis.

More recently, the use of polymeric NHC ligands has emerged as a versatile platform for stabilizing nanoparticles and controlling interfacial environments. Studies by He and co-workers in 2019 and 2023 showed that Au and Pd NPs modified with polydentate or amphiphilic NHC-containing polymers exhibited greatly improved durability (86% activity retention over 11 h) and enhanced CO selectivity [36]. In the 2019 study, a polystyrene-based NHC polymer (PIL-Im) was employed to functionalize Au and Pd nanoparticles, yielding catalysts that not only prevented metal nanoclustering but also displayed up to a twofold enhancement in CO selectivity compared to unmodified particles (Figure 4c). Operando ATR–SEIRAS measurements revealed suppressed surface-bound H species, explaining the decreased H_2 evolution. Notably, Pd@PIL-Im reached a CO Faradaic efficiency of 83% at −0.9 V vs. RHE, a substantial improvement over Pd-only catalysts. In the 2023 work, the group introduced a library of amphiphilic poly(NHC) ligands containing hydrophobic alkyl spacers and hydrophilic ionic backbones. This architecture facilitated controlled assembly on Pd surfaces and altered the local environment around the metal interface. The hydrophobic domains were shown—via molecular dynamics simulations and spectroscopic evidence—to exclude interfacial water and promote local CO_2 enrichment. The most optimized Pd@polyNHC catalyst achieved a turnover frequency (TOF) of 3200 h^{-1} at −0.85 V vs. RHE, with high stability and negligible metal leaching. The hydrophobic segments of the polymers were found to influence water structure near the surface, suppressing competing hydrogen evolution and enriching local CO_2 concentration. These “soft-shell” catalysts mimic aspects of metalloenzyme environments, demonstrating how synthetic ligands can sculpt microenvironments to favor CO_2 activation.

A recent study reported NHC–polymer stabilized Au nanowires as highly selective and morphologically robust CO_2RR catalysts (Figure 4d) [37]. In this system, ultrasmall Au nanowires (~3.8 nm diameter, up to 1.5 μm long) were stabilized by polystyrene chains terminated with imidazolium groups, which were converted in situ to surface-anchored NHCs through electrochemical activation. The imidazolium-terminated polystyrene chains provided both strong Au–NHC anchoring and hydrophobic polymeric microenvironments, enabling >90% CO selectivity across a wide potential window (−0.4 to −1.0 V vs. RHE) and a mass activity of 142 $A \cdot g^{-1}_{Au}$, among the highest reported for Au-based CO_2RR catalysts. In situ ATR-IR spectroscopy confirmed a suppressed HER signal and enrichment of local CO_2 near the electrode surface, validating the microenvironment effect. These nanowires also demonstrated excellent structural integrity during extended electrolysis (>12 h), with negligible loss of activity or morphology. Furthermore, they were successfully integrated into a tandem flow cell with Cu nanowires, achieving 58% FE toward C_2H_4, showcasing their utility in multi-step CO_2 conversion schemes. This work exemplifies how NHC-based polymer architectures can optimize both catalyst performance and stability under harsh electrochemical conditions, and how modular organic shells can be precisely tuned to mimic enzyme-like active site environments.

2.2.2. Copper

In another significant recent advance, copper electrodes functionalized with NHC-carbodiimide (NHC–CDI) ligands have shown dramatic increases in multicarbon product formation compared to bare Cu [38]. This study by Rosas-Hernández and co-workers reported that an NHC–CDI modified Cu catalyst produced C_2^+ products at more than an order of magnitude higher rate than an unmodified Cu surface. These hybrid Cu–NHC electrodes operated efficiently in a gas-diffusion electrolyzer, reaching partial current densities for C_2^+ products up to ~–80 mA·cm^{-2} with 58% FE toward C_2^+ (ethylene, ethanol, etc.) and a total current density of −121 mA·cm^{-2} at −0.94 V vs. RHE. The catalyst exhibited stable operation for at least 10 h, maintaining high FE and selectivity. Mechanistic probes (XPS and in situ Raman) revealed that the NHC–CDI ligands altered the Cu surface electronic structure, increasing the steady-state coverage of *CO intermediates and shifting the onset potential for CO formation positively. In particular, the modifiers helped stabilize CO on undercoordinated Cu step sites—known to be the active sites for C–C coupling—thereby steering the reaction toward multi-carbon products. Density functional theory (DFT) further supported this mechanism, showing that NHC–CDI ligands lower the energy barrier for CO dimerization and stabilize adsorbed *CO intermediates. This is a clear example of how molecular design at an electrode interface can redirect the intrinsic selectivity of a metal catalyst, achieving higher-order CO_2 reduction products that are otherwise difficult to obtain on unmodified Cu. The work also highlights the potential of CDI moieties in tailoring surface binding geometries, suggesting new avenues for ligand-assisted C–C coupling on earth-abundant metal catalysts.

2.3. Atomically Precise NHC-Stabilized Metal Nanoclusters

NHC ligands have also been employed to stabilize atomically precise metal nanoclusters—systems that bridge the gap between discrete molecules and bulk materials while retaining well-defined crystallographic structures. In 2019, Crudden and co-workers reported the first NHC-stabilized gold(0) nanoclusters [39]. They synthesized magic-number Au clusters bearing NHC ligands by reducing NHC–Au(I) precursors. Even the addition of a single NHC ligand to a thiolate-protected gold cluster was found to significantly improve the cluster's stability and electrocatalytic CO_2 reduction performance. By tuning the reaction conditions and NHC equivalents, they obtained predominantly monosubstituted clusters (one NHC per nanocluster) and even mixtures with up to five NHCs bound. This series of NHC-functionalized clusters revealed a clear trend: catalytic performance correlated with cluster stability. The most stable (resistant to agglomeration and oxidation) NHC–Au_{11} cluster (with 3 NHCs) showed the highest CO FE, mass activity, and current density among all clusters tested. In contrast, less-stable analogues (e.g., with fewer or no NHCs) showed diminished performance.

Building on this concept, a later study by Tang and co-workers in 2025 demonstrated that $[Au_{13}(NHC)_9Cl_3]^{2+}$ clusters undergo partial electrochemical dechlorination under reducing conditions, activating the underlying Au core for CO_2 electroreduction [40]. Constant potential AIMD simulations and XPS measurements revealed that Cl ligands are selectively stripped while the NHC–Au interface remains intact. This controlled ligand etching exposes undercoordinated Au sites capable of catalyzing syngas ($CO + H_2$) formation with a tunable $CO:H_2$ ratio between ~0.8–1.2 across a broad potential range. In short, the strong Au–C bond of NHCs endowed these clusters with greater thermal and electrochemical stability than traditional thiolate- or phosphine-stabilized clusters, and this stability translated to better sustained activity in CO_2 electroreduction.

In parallel, Crudden's team developed hydrido Au_{24}(NHC) nanoclusters in 2022, which feature two joined Au_{12} kernels bridged by hydride ligands (Figure 4e) [41]. These systems displayed sustained activity and high selectivity for CO production under electrochemical conditions, achieving Faradaic efficiencies of ~85% at −0.8 V vs. RHE in $KHCO_3$. Spectroscopic and crystallographic analyses confirmed that the hydride ligands bridge the two Au_{12} icosahedra, enabling dynamic fluxionality and partial electron delocalization. This structural adaptability may stabilize reactive intermediates and facilitate charge redistribution. Post-electrolysis characterization showed the nanocluster remained largely intact, underscoring the stabilizing role of the Au–NHC interface.

Most recently, the same team presented bis-NHC–stabilized Au_{13} clusters, which have been shown to excel as CO_2RR catalysts after a strategic activation step (Figure 4f) [42]. In these systems, each Au_{13} cluster is protected by several bidentate NHC ligands ("bis-NHCs") instead of monodentate carbenes. When supported on carbon and tested for CO_2 electroreduction, the as-synthesized bis-NHC Au_{13} clusters already exhibited high CO selectivity; but significantly, upon mild thermal activation, their performance further improved beyond that of analogous phosphine-stabilized Au_{13} clusters. Thermogravimetric and XPS studies revealed why: heating caused a partial ligand removal in the bis-NHC clusters—some NHC ligands detached, creating open active sites on the Au_{13}, whereas the cluster core remained intact. In contrast, diphosphine-protected Au_{13} clusters lost all their ligands under the same treatment, essentially degrading to larger particles or unligated clusters. The partially de-ligated NHC clusters achieved Faradaic efficiencies for CO up to ~92%, significantly higher than the diphosphine

analogues. This result suggests that maintaining cluster integrity while exposing some active surface is critical—a balance that NHC ligands can achieve due to their strong binding. Indeed, the partially ligand-stripped $Au_{13}(NHC)_5Cl_2$ clusters were far more active than completely ligand-free clusters, underscoring that a "ligand-on" strategy (with the right amount of ligand) can outperform a complete ligand removal. In essence, the robust bis-NHC shell prevents sintering but is labile enough to open sites for reaction, illustrating a powerful design principle for cluster catalysts.

Collectively, these studies illustrate that the ligand shell is not a passive bystander in nanocluster catalysis—its thermal stability, rigidity, and electronic character all influence the cluster's structure and reactivity. NHC ligands, with their tunable sterics and strong σ-donor ability, offer a unique handle on these parameters and open the door to rationally designing robust, well-defined nanocatalysts for CO_2RR. By adjusting ligand coverage or backbone, one can tune the availability of active metal sites and the cluster's resistance to deactivation in tandem. This level of control is difficult to achieve with traditional thiolate or phosphine ligands, highlighting a key advantage of NHCs in the quest for efficient CO_2 conversion.

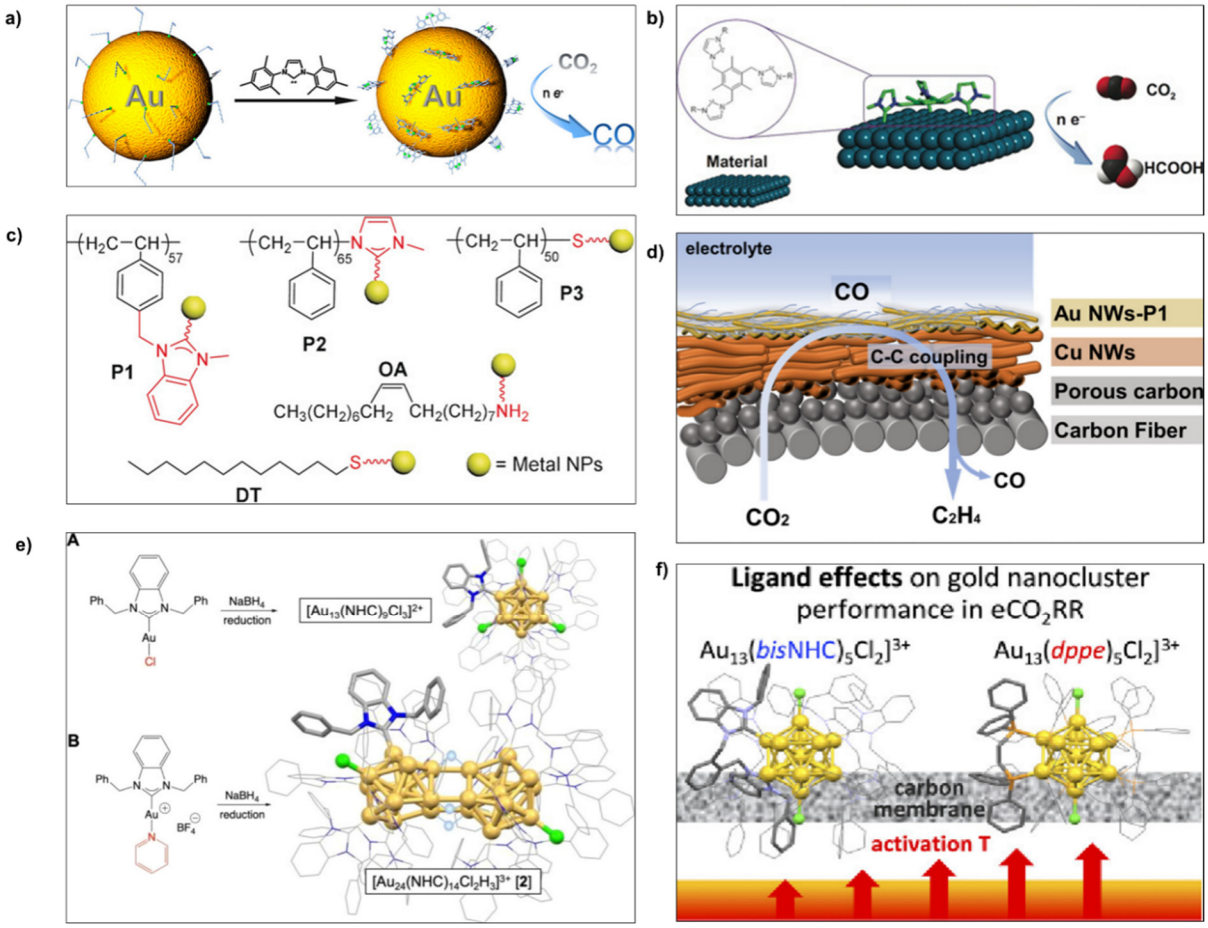

Figure 4. NHC-based hybrid CO_2RR electrocatalysts: (**a**) NHC carbene-functionalized Au NPs prepared through ligand exchange reaction. Reproduced from [33] with permission from the American Chemical Society, (**b**) Palladium foil functionalized with a chelating tris-N-heterocyclic carbene ligand. Reproduced from Ref. [35] with permission from the Wiley-VCH GmbH, (**c**) AuNPs and PdNPs modified with five different polymeric ligands (P1 and P2 are NHC-based). Reproduced from Ref. [36] with permission from the Wiley-VCH GmbH, (**d**) Au NWs modified with P1 (methylimidazolium-terminated polystyrene). Reproduced from Ref. [37] with permission from the American Chemical Society, (**e**) Au_{13}(NHC) cluster and hydrido-bridged Au_{24}(NHC) nanocluster formed via $NaBH_4$ reduction of Au–NHC halide and Au–NHC pyridine precursors, respectively. Reproduced from Ref. [41] with permission from the American Chemical Society, (**f**) Thermally activated Au_{13} nanoclusters stabilized by bis-NHC or dppe ligands on carbon membrane, illustrating ligand-dependent CO_2RR performance. Reproduced from Ref. [42] with permission from the American Chemical Society.

2.4. Concluding Remarks on CO_2 Electroreduction

To distill the mechanistic insights described above into broader design principles, Table 2 summarizes the central structural motifs in NHC–metal CO_2RR electrocatalysts, their mechanistic consequences, and representative performance anchors.

Table 2. Structural–performance correlations in NHC–metal CO_2RR electrocatalysts.

Structural Motif/Design Strategy	Mechanistic Consequence	Performance Anchor	Ref.
Strong σ-donation (Mn–NHC, Fe tetracarbene)	Compresses reduction potentials; stabilizes metal-centered radicals	TOF up to 3.2×10^5 s^{-1} (Mn bis-NHC)	[20]
Mixed donors (Fe–tpy–bisNHC, Pd–bisNHC)	Redox buffering without displacing metal activity	Low overpotential $\eta \approx 0.2$ V (Fe–tpy–bisNHC)	[22]
Geometric rigidity (cis-Ni C, O chelates; rigid Mn/Co backbones; macrocyclic Co)	Promotes orbital alignment, hydride formation, lowers η, and prevents deactivation	FE(formate) ≈ 83% (Ni cis isomer); $\Delta\eta = -190$ mV (Mn Ph-bis-mim); FE(CO) ~98% (Co rigid macrocycle)	[15,21,26]
Hemilabile dynamics (Fe–pyridyl-NHC)	Enables reversible CO release, avoids product inhibition	FE(CO) > 95% at $\eta \approx 0.15$ V	[23]
Hydrophobic polymeric/amphiphilic shells (Au, Pd NPs; Au nanowires)	Exclude water, enrich CO_2, suppress HER; mimic enzyme-like environments	FE(CO) 83% (Pd@PIL-Im); TOF 3200 h^{-1} (Pd@polyNHC); FE(CO) >90% (Au nanowires)	[36,37]
Carbodiimide modifiers (Cu–NHC–CDI)	Stabilize *CO at step sites, promote C–C coupling	FE(C_2^+) 58% at −0.94 V, j ≈ −80 mA cm^{-2}	[38]
Atomically precise clusters (Au_{13}, Au_{24})	NHCs balance stability with active site exposure; partial ligand removal activates sites	FE(CO) 92% (bis-NHC–Au_{13}); FE(CO) 85% (Au_{24} hydrides)	[41,42]

2.4.1. Metal- vs. Ligand-Centered Reduction—Mn vs. Re Pincers as a Design Principle

A recurring debate in CO_2RR catalysis concerns whether reduction should localize on the metal or delocalize onto the ligand framework. Bis-NHC pincer complexes of Mn and Re starkly illustrate this issue. In the Mn(I) system, the one-electron reduced state is a metal-centered radical (Mn^0) with ~66% spin density on Mn. This radical is highly nucleophilic, binds CO_2 readily, and drives selective CO formation with high turnover. In contrast, the Re analogue forms a ligand-centered radical, with only ~38% spin on Re. Here, the Re atom behaves almost as a closed shell, binding CO_2 weakly and showing negligible catalytic turnover.

The broader implication is that excessive charge delocalization onto redox-active ligands can undermine reactivity, even while stabilizing the complex. Effective CO_2RR requires a balance: ligands may buffer electrons to prevent decomposition, but the reduced state must retain sufficient metal-centered character to engage CO_2. This mechanistic dichotomy—nucleophilic metalloradical vs. ligand-based radical—provides a critical design lens for future NHC architectures.

2.4.2. Overall Concluding Remarks

Taken together, the studies above survey the landscape of molecular and hybrid NHC–metal electrocatalysts for CO_2 reduction. They illustrate several key design strategies:

(1) Strong σ-donation and modular electronics. NHCs enhance metal electron density, promoting CO_2 activation and enabling multi-electron pathways. Their tunability allows fine control of both electronics and sterics, while mechanistic contrasts (Mn vs. Re pincers) underscore the importance of keeping reduction localized at the metal center.

(2) Mixed-donor and redox-active ligand environments. Pairing NHCs with pyridyl or terpyridine donors stabilizes reduced states while preserving metal reactivity, enabling low overpotentials. Excessive ligand delocalization, however, can limit substrate binding, whereas well-balanced frameworks (e.g., Fe–tetracarbene, Fe–tpy–bisNHC) sustain efficient CO_2 reduction.

(3) Rigidity vs. hemilability. Rigid NHC scaffolds (cis Ni chelates, Mn/Co backbones, Co macrocycles) enforce geometries that lower overpotential and prevent deactivation, while hemilabile motifs (pyridyl–NHCs) provide enzyme-like flexibility that facilitates product release and mitigates inhibition.

(4) Microenvironmental design. NHC-containing polymers and amphiphilic shells introduce hydrophobic domains that enrich CO_2 and suppress HER, demonstrating that secondary-sphere control is as critical as primary coordination in steering selectivity.

(5) Stability and durability. NHC–metal bonds withstand electrochemical stress better than phosphines or amines, preventing agglomeration and maintaining activity under prolonged cycling. In nanocluster systems, partial but controlled ligand removal illustrates how NHCs can balance stability with exposure of active sites.

Looking forward, these principles establish NHC ligands as versatile tools in advancing CO_2RR. Their ability to combine electronic control, geometric rigidity/flexibility, enzyme-like microenvironments, and long-term stability positions them as unique platforms for designing next-generation molecular and hybrid catalysts. Indeed, some of the most selective and durable CO_2RR catalysts to date—spanning Ni, Mn, Fe, Co, and Au—derive their performance directly from NHC design. The next step lies in translating these strategies to practical systems, bridging molecular precision with scalable hybrid architectures that integrate NHCs into conductive surfaces and membranes for real-world CO_2 electrolysis.

3. Hydrogen Evolution Reaction (HER)

The application of NHC-based systems in electrocatalytic HER has gained increasing attention in recent years, with several studies demonstrating the ability of NHC ligands to enhance HER performance through electronic and structural tuning. The most extensive and systematic investigations have been reported by Budagumpi and co-workers, who developed a broad range of mono- and bis-NHC metal complexes, often incorporating coumarin-functional groups and spanning various transition metals. Complementing these efforts, Wang et al. conducted a mechanistic study of Ni(II) complexes bearing C_2-symmetric NHC–amidate ligands, highlighting how redox behavior and HER activity correlate with ligand electronics through proton-coupled electron transfer sequences. Choudhury's group introduced a hydrogenase-inspired Co(III)–NHC complex featuring a pendant pyridinone base that acts as an intramolecular proton relay, achieving one of the highest TOF_{max} values reported for cobalt HER catalysts in non-aqueous media. At the nanoscale, Brutchey et al. developed NHC-capped $Cu_{3-x}P$ nanocrystals, and Rapakousiou et al. engineered MWCNT–NHC–Pt hybrid materials with ultra-low Pt loadings, demonstrating high specific activity and long-term stability. Together, these studies underscore the versatility of NHCs in tuning both molecular and hybrid architectures for efficient hydrogen evolution catalysis.

3.1. NHC-Metal-Based HER Electrocatalysts

One early example demonstrated NHC-ligated copper phosphide ($Cu_{3-x}P$) nanocrystals, prepared by reacting an NHC–Cu precursor with tris(trimethylsilyl)phosphine (Figure 5a) [43]. Brutchey and co-workers showed that these NHC-capped $Cu_{3-x}P$ nanocrystals had significantly improved HER activity versus oleylamine-capped analogues, which was attributed to favorable surface electronic effects induced by the NHC ligands. Electrochemical measurements in 0.5 M H_2SO_4 on glassy carbon revealed that the NHC–$Cu_{3-x}P$ nanocrystals required an overpotential of 450 mV to reach −10 mA cm^{-2}, significantly lower than the 860 mV needed for the OA–$Cu_{3-x}P$ counterpart (Table 3, entry 1). Similarly, the Tafel slope of 85 mV dec^{-1} indicates enhanced HER kinetics with NHC ligation, surpassing the OA–$Cu_{3-x}P$ by 143 mV/dec. Density functional theory (DFT) calculations suggested that NHC capping reduces the surface electrostatic potential near proton-accessible sites, thereby minimizing repulsive interactions and facilitating proton adsorption on the $Cu_{3-x}P$ surface. This study underscored that even at inorganic surfaces, strongly bound carbenes can modulate surface charge and binding characteristics in ways beneficial for proton reduction. Moreover, the NHC–$Cu_{3-x}P$ catalyst demonstrated stable current output over 6 h of chronopotentiometric testing, confirming the durability conferred by robust NHC surface anchoring.

Another notable avenue has been the development of molecular NHC–metal complexes as HER catalysts, led prominently by Budagumpi and co-workers. In an initial study, they synthesized a family of Ag(I), Au(I), and Ni(II) complexes supported by coumarin-derived NHC ligands (including mono- and bis-NHC coordination) [44]. When immobilized on glassy carbon electrodes in acidic media, several of these complexes showed promising HER activity—for example, bis-NHC Ag(I) complexes required overpotentials around −230 to −240 mV (to reach 10 mA cm^{-2}), substantially lower than their mono-NHC analogues, and a mono-NHC Au(I) complex outperformed its Ag counterpart (∼−310 mV vs. −445 mV) despite similar coordination geometries (Table 3, entries 2–5). However, the stability of these complexes proved moderate by the loss of overpotentials after multiple cycles (52 mV—353 mV loss), with the most stable ones being the mono-substituted ones. The Tafel slopes (typically 100–270 mV/dec) and exchange current densities (up to ~1 μA cm^{-2}) indicated a Volmer–Heyrovsky mechanism in most cases, with the NHC ligand environment influencing the proton adsorption step. DFT calculations for this series confirmed an unexpected ligand-centered HER pathway: the active site for hydrogen binding was a specific carbon on the NHC

ligand rather than the metal center. This ligand-centric behavior, enabled by the strong σ-donor character of NHCs, was a recurring theme in subsequent studies and highlighted how NHCs can act as proton-responsive sites in addition to stabilizing the metal.

The same group then developed a series of mono- and bis-NHC–palladium(II) complexes bearing coumarin-functionalized NHC ligands, which were investigated as electrocatalysts for the hydrogen evolution reaction (HER) under acidic conditions [45]. Six Pd(II) complexes with different substituted benzo-coumarin were synthesized and immobilized on glassy carbon electrodes. Among them, the bis-5,6-benzo-coumarin and mesityl-substituted bis-NHC Palladium(II) complex exhibited the best HER performance, achieving an overpotential of −347 mV at 10 mA/cm^2 in 0.5 M H_2SO_4, a Tafel slope of 113 mV/dec, and a turnover frequency (TOF) of 10.1 s^{-1} (Table 3, entry 6). Additionally, the bis-NHC ligated complexes generally surpassed their mono-NHC analogs, suggesting that bidentate NHC coordination improves catalyst stability and electronic properties. Faradaic efficiencies (up to 98%) and long-term durability (chronoamperometric measurement up to 10 h) further confirmed the viability of these molecular Pd–NHC complexes. This work shows a mediocre HER performance but highlights the role of ancillary ligand design and chelation in optimizing HER activity for Pd-based molecular systems. Building on previous work with coumarin-functionalized NHC ligands, the same group. synthesized and evaluated a series of mono- and bis-NHC complexes of Ni(II), Ag(I), and Au(I) with methyl and chloro substituents for HER in acidic media [46]. The electrocatalysts were drop-cast on glassy carbon electrodes and tested in 0.5 M H_2SO_4. Among these, the chlorocoumarin and mesityl-substituted NHC-Ag(I)Br mono complex showed some electrocatalytic activity with η_{10} = 298 mV and a Tafel slope of 70 mV/dec; however, the charge transfer resistance of 625 Ω shows that it's not a kinetically favorable reaction process (Table 3, entry 7). Again, in a complementary study focused solely on nickel systems, Budagumpi and co-workers synthesized a water-soluble macrocyclic bis-NHC Ni(II) complex [47]. It showed some electrocatalytic activity in both aqueous and organic media, with authors reporting that it delivered 165 μmol H_2 over 11 h with 98% Faradaic efficiency at 0.888 V overpotential. This system also exhibited a reversible Ni(II)/Ni(I) redox couple.

Expanding the scope of NHC–metal systems for HER, Budagumpi and co-workers also reported a comparative study of Ru(II) and Ag(I) complexes. Specifically, they synthesized through a transmetallation reaction from a coumarin-substituted bis-NHC-Ag(I) complex, a secondary butyl and benzannulated coumarin-substituted 1,2,4-Triazole-Ru (II)-cymene complex which showed efficient activity in HER (Figure 5b) [48]. The NHC-Ru complex showed an overpotential of 175 mV at −10 mA/cm^2 and a low Tafel slope (94 mV/dec) and charge-transfer resistance (125Ω) (Table 3, entry 8). Despite using a noble metal, this study demonstrates how ligand design and electronic tuning can yield efficient, well-defined molecular HER catalysts with potential for integration into electrochemical technologies. Progressing further in coumarin-substituted NHC–Pd electrocatalysts, the same group synthesized a new series of mono- and bis-coumarin and allyl-substituted NHC–Pd(II) complexes and evaluated their HER performance in 0.5 M H_2SO_4 [49]. The sterically hindered bis-NHC–Pd(II) complexes, featuring square-planar geometry with Pd–π and Pd–HC interactions, were structurally characterized in detail. In HER testing, the bis-(5,6-benzo-coumarin and allyl-substituted 1,2,4-triazol-5-ylidene) Pd(II) complex and its mesoporous carbon composite achieved overpotentials of 570 mV and 468 mV at −10 mA cm^{-2}, with Tafel slopes of 187 and 161 mV/dec and charge transfer resistances of 68 and 58 Ω, respectively (Table 3, entries 9 and 10). Both followed a Volmer–Heyrovsky mechanism and exhibited high stability, with the carbon composite retaining ~92% of its initial current after 12 h of HER testing. Hydrogen evolution was independently confirmed by synchronized disk and ring responses in RRDE measurements. At the same time, FT-IR analysis before and after electrolysis indicated that the molecular structure of the electrocatalyst remained intact. The improved performance of the carbon composite was attributed to enhanced π-electron delocalization, which facilitated more efficient electron transfer.

In 2024, an interesting mechanistic study for probing how ligand electronics govern redox behaviour and proton-reduction catalysis was reported by Wang and co-workers. They prepared three neutral Ni(II) complexes bearing C_2-symmetric tetradentate NHC–amidate ligands with varied electronic substituents [50]. Cyclic voltammetry in MeCN showed a reversible Ni(II)/Ni(I) wave that shifted cathodically from −2.52 V to −2.60 V vs. Fc/Fc$^+$, mirroring the increasing electron-donation of the amidate moiety. In the presence of TFA, each complex followed an ECEC sequence (E = electrochemical step, C = chemical step), and catalytic currents grew linearly with acid concentration; corresponding TOFs rose from 316 s^{-1} < 409 s^{-1} < 698 s^{-1}, while overpotentials decreased from 780 mV to 760 mV, upon increase of electron donation from the ligand. The data indicate that the most electron-rich complex, which displays the most positive Ni(II)/Ni(I) redox potential, delivers the fastest HER turnover at the lowest driving force. Electrochemical analysis supports a cycle in which Ni(II) is reduced to Ni(I), protonated to a Ni(III)–H species, further reduced to Ni(II)–H, and then protonated (or dimerized) to release H_2, regenerating Ni(II). These results highlight how fine-tuning ligand electronics in NHC-amidate frameworks can systematically improve the activity and efficiency of base-metal molecular HER catalysts.

In a recent advance, Budagumpi and co-workers synthesized a series of mono- and tri-nuclear NHC–metal complexes, including a Au(I) chlorido monocarbene complex (AuLCl) and trinuclear Ag(I) and Au(I) tricarbene metallacycles ($Ag_3L_3 \cdot 3PF_6$ and $Au_3L_3 \cdot 3PF_6$), and evaluated their HER activity in alkaline media after deposition onto carbon cloth (CC) via dip-coating (Figure 5c) [51]. While the mononuclear AuLCl exhibited negligible activity, both metallacycles demonstrated measurable HER performance, with $Ag_3L_3 \cdot 3PF_6$ and $Au_3L_3 \cdot 3PF_6$ reaching overpotentials of 473 and 485 mV at −10 mA/cm^2, respectively (Table 3, entries 11 and 12). Notably, incorporation of conductive carbon ink led to significant improvements, reducing overpotentials to 187 mV and 416 mV for $Ag_3L_3 \cdot 3PF_6$/C and $Au_3L_3 \cdot 3PF_6$/C, respectively, and lowering Tafel slopes (169 and 313 mV/dec). The Ag complex, featuring extended π-systems, also adhered to the CC surface -without binders- via π–π stacking and exhibited excellent operational durability over 24 h. While partial deactivation was observed due to complex leaching, structural integrity was retained, highlighting the promise of π-conjugated NHC metallacycles for the design of molecularly anchored, free-standing HER electrodes.

In a significant advance toward base-metal HER catalysis, Choudhury and co-workers introduced a hydrogenase-inspired cobalt(III) complex, Co–NHCU, which combines a strong σ-donor NHC ligand with a pendant anionic uracil-derived pyridinone moiety acting as a proton shuttle adjacent to the cobalt center (Figure 5d) [52]. Mimicking the function of the pyridinol unit in [Fe]-hydrogenase, this structural design enables efficient intramolecular proton-coupled electron transfer (PCET) and facilitates hydride/proton coupling for H_2 evolution. The system exhibits exceptional electrocatalytic HER activity in non-aqueous media with various proton sources, reaching turnover frequencies (TOF_{max}) as high as 13,700 s^{-1} and Faradaic efficiencies of 93–98% at overpotentials of 0.50–0.78 V (Table 3, entry 13). Mechanistic studies reveal that the pyridinone group participates in a stepwise protonation and reduction sequence, forming a Co–H species that undergoes rate-limiting intramolecular dihydrogen elimination via adjacent pyridinol–OH coupling. This carefully engineered interplay between electronic modulation by the NHC and proton relaying by the pendant base results in one of the highest TOF_{max} values reported for cobalt HER electrocatalysts under non-aqueous conditions. The study underscores the untapped potential of biomimetic design—particularly the integration of pyridinone-type proton shuttles with Earth-abundant NHC-metal frameworks—for developing next-generation homogeneous HER systems with high efficiency and mechanistic fidelity.

Apart from molecular complexes, NHCs have also been used to engineer hybrid nanomaterial catalysts for HER. A striking example is a study by Rapakousiou and co-workers, who constructed a multi-walled carbon nanotube (MWCNT) supported Pt nanocatalyst with NHC linkers [53]. In this system, NHCs bearing triazole anchors were covalently grafted on MWCNTs and used to nucleate and bind ultrasmall Pt(0) nanoparticles (~2 nm, {111}-faceted PtNPs) (Figure 5e). The resulting MWCNT–NHC–Pt material achieved an overpotential of 77 mV at −10 mA cm^{-2} with a Tafel slope of 50 mV/dec (Table 3, entry 14). Although commercial Pt/C (20 wt%) under identical conditions exhibits slightly superior absolute performance (E_{10} = 34 mV; Tafel slope = 19 mV/dec), the NHC–Pt catalyst contains only 0.4 at% Pt. When normalized to the electroactive surface area, the specific activity at 100 mV overpotential reaches 15 mA cm$^{-2}{}_{Pt}$, which is approximately three times higher than Pt/C, increasing to 53 mA cm$^{-2}{}_{Pt}$ at 200 mV. This performance range, extending to high current densities, supports the practical relevance of the system for scaled HER applications. The enhanced per-atom efficiency underscores the impact of NHC coordination in maximizing noble metal utilization. Furthermore, the mass activity reached 8.6 A/mg$_{Pt}$ at 200 mV overpotential, reflecting highly efficient utilization of each single Pt site. The NHC ligands were found to play a dual role: (i) promoting a uniform dispersion of small, crystalline PtNPs and (ii) modifying the Pt surface electronic structure to resist oxidation and aggregation. Indeed, cyclic voltammetry revealed a well-defined and reversible Pt^0/Pt^{2+} redox couple, indicative of surface-confined, diffusion-assisted charge storage behavior. This suggests that the NHC ligands stabilize the electron-rich Pt (0) surface, thereby facilitating proton reduction. Notably, the NHC-bound PtNPs retained their activity without exhibiting the rapid deactivation, typically associated with surface oxide formation, leading to remarkable stability over extensive cycling. This hybrid approach demonstrates how NHCs can be leveraged in heterogeneous catalysis to stabilize ultra-low loadings of noble metals, potentially lowering cost while maintaining ultrahigh activity. It also highlights the versatility of NHC chemistry: from serving as surface capping agents on colloidal nanocrystals to acting as covalent linkers in electrode materials, NHCs provide robust metal–carbon interfaces that traditional surfactants or thiols often cannot match in stability.

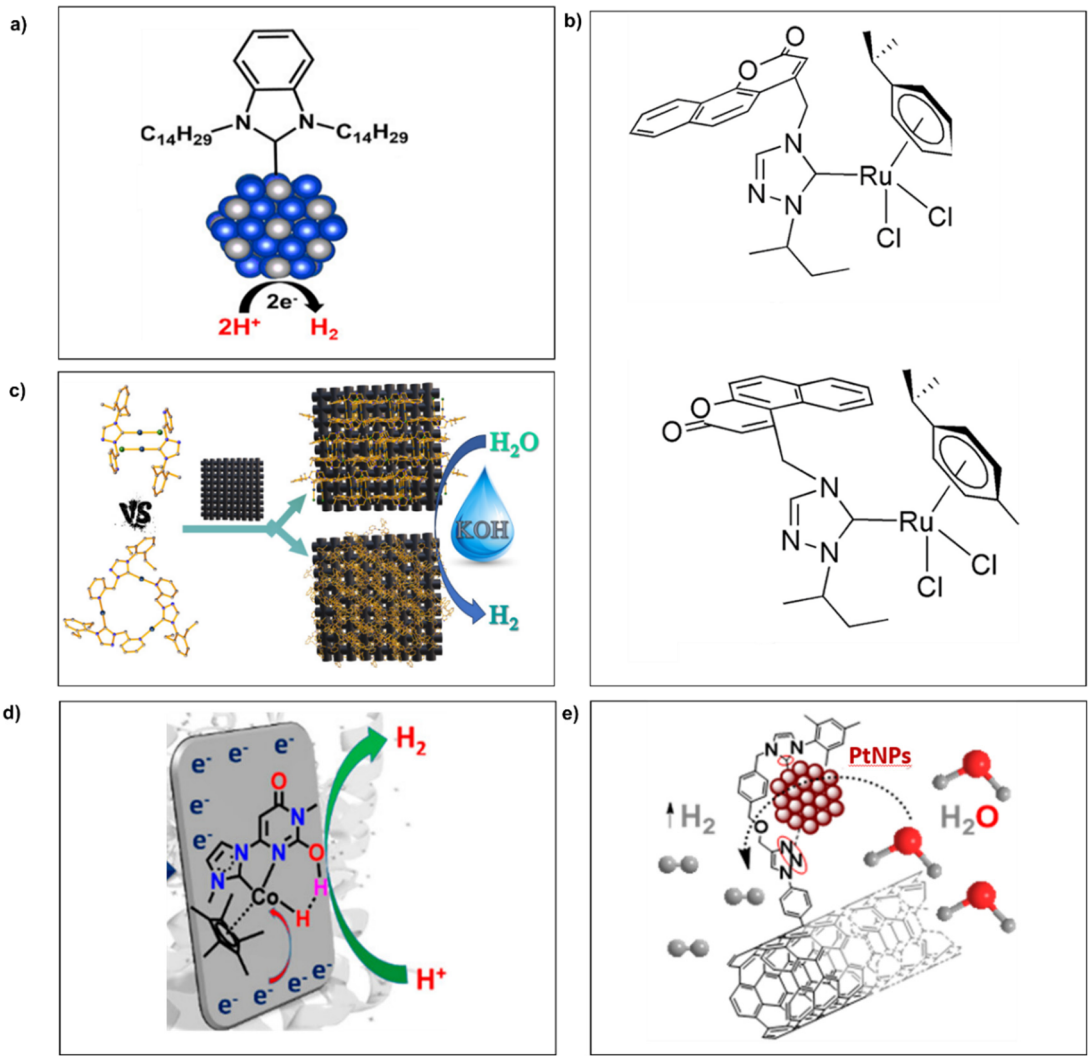

Figure 5. NHC-based electrocatalysts for HER: (**a**) NHC-ligated $Cu_{3-x}P$ nanocrystals showing superior performance to the as compared to oleylamine-ligated $Cu_{3-x}P$ catalysts. Reproduced from Ref. [43] with permission from the American Chemical Society, (**b**) Secondary butyl and 7,8-benzannulated coumarin-substituted 1,2,4-triazole-Ru (II) complexes prepared by in situ deprotonation of triazolium salt analogues. Reproduced from Ref. [48] with permission from the American Chemical Society, (**c**) Au(I) Chlorido Mono-carbene Complex (AuLCl), Tri-nuclear Ag(I) Tri-carbene Metallacycle ($Ag_3L_3{\cdot}3PF_6$), and Tri-nuclear Au(I) Tri-carbene Metallacycle ($Au_3L_3{\cdot}3PF_6$) deposited as distinct, fine microgranules with varying sizes and shapes, on carbon cloth electrode. Reproduced from Ref. [51] with permission from the American Chemical Society, (**d**) Co-based complex Co–^{NHC}U, containing an anionic uracil nucleobase, connected with a strong sigma-donor NHC, wherein the anionic uracil motif offers a pyridinone-type proton-responsive site adjacent to the Co center. Reproduced from Ref. [52] with permission from the American Chemical Society, (**e**) MWCNTs-NHC-PtNPs forming robust covalent bonds with highly crystalline ~2 nm PtNPs. Reproduced from Ref. [53] with permission from the American Chemical Society.

Table 3. NHC-based electrocatalysts for HER.

	NHC-Metal System	Conditions	η_{10} (mV)	Tafel Slope (mV/dec)	Rct (Ω)	Ref.
1	**NHC-ligated $Cu_{3-x}P$ nanocrystals**	0.5 M H_2SO_4, Glassy carbon	450	85	20	[43]
2	**7,8-benzo-coumarin and mesityl-substituted bisNHC-Ag (I)**	0.5 M H_2SO_4, Glassy carbon	226	96	-	[44]
3	**5,6-benzannulated coumarin and mesityl-substituted NHC-Ag (I)Br**	0.5 M H_2SO_4, Glassy carbon	445	271	-	[44]
4	**7,8-benzannulated coumarin and mesityl-substituted bisNHC-Ag (I)**	0.5 M H_2SO_4, Glassy carbon	243	108	-	[44]
5	**5,6-benzo-coumarin and mesityl-substituted NHC-Au (I)Cl**	0.5 M H_2SO_4, Glassy carbon	310	211	-	[44]

Table 3. *Cont.*

	NHC-Metal System	Conditions	η_{10} (mV)	Tafel Slope (mV/dec)	Rct (Ω)	Ref.
6	**Bis-5,6-benzo-coumarin and xylyl-substituted 1,2,4-triazole-5-Pd(II)**	0.5 M H_2SO_4, Glassy carbon	534	190	~40	[45]
7	**Chlorocoumarin and mesityl- substituted NHC-Ag(I)Br**	0.5 M H_2SO_4, Glassy carbon	298	70	625	[46]
8	**Secondary butyl and 7,8-benzannulated coumarin-Substituted 1,2,4-triazole-Ru (II)**	0.5 M H_2SO_4, Glassy carbon	175	94	125	[48]
9	**Bis-5,6-benzo-coumarin and allyl-substituted 1,2,4-triazole-5-Pd(II)**	0.5 M H_2SO_4, Glassy carbon	570	187	68	[49]
10	**Bis-5,6-benzo-coumarin and allyl-substituted 1,2,4-triazole-5-Pd(II)/ mesoporous carbon composite**	0.5 M H_2SO_4, Glassy carbon	468	161	58	[49]
11	**$Ag_3L_3{\cdot}3PF_6$/$Ag_3L_3{\cdot}3PF_6$/C**	1 M KOH Carbon cloth	473/187	319/169	72/10	[51]
12	**$Au_3L_3{\cdot}3PF_6$/ $Au_3L_3{\cdot}3PF_6$/C**	1 M KOH Carbon cloth	485/416	329/313	77/48	[51]
13	**Co−NHCU**	CH3COOH (500 mM), 0.1 (M) Bu4NPF6, glassy carbon	500	-	-	[52]
14	**MWCNTs-NHC-Pt (0)NPs**	0.5 M H_2SO_4, Glassy carbon	77	50	90	[53]

3.2. Concluding Remarks on HER

To extract unifying principles from the diverse examples above, Table 4 outlines the key structural motifs explored in NHC–metal HER electrocatalysts, linking each to its mechanistic consequence and representative performance. This framework emphasizes how NHC ligands stabilize metal(0) centers under reductive conditions, introduce alternative ligand-centered pathways, and enable enzyme-like proton relays or hybrid interfacial environments that critically determine catalytic efficiency and durability.

Table 4. Structural–performance correlations in NHC–metal HER electrocatalysts.

Structural Motif/Design Strategy	Mechanistic Consequence	Performance Anchor	Ref.
Strong σ-donation & stabilization of M^0 (Ni–NHC amidates, MWCNT–NHC–Pt, $Cu_{3-x}P$)	Maintains reduced metal(0) centers under cathodic bias; critical for sustained HER	η_{10} = 77 mV, mass activity 8.6 A/mg_{Pt} (MWCNT–NHC–Pt); η_{10} = 450 mV ($Cu_{3-x}P$); TOF = 698 s^{-1} (Ni–amidate)	[43,50,53]
Ligand-centered H binding (Ag, Au coumarin–NHCs)	HER proceeds at the carbene carbon site; Volmer–Heyrovsky mechanism	η_{10} ≈ 230–310 mV, FE up to 98%	[44]
Proton relays/pendant bases (Co–NHCU with pyridinone)	Intramolecular proton shuttle enables rapid PCET, mimicking hydrogenase	TOFmax = 13,700 s^{-1}, FE 93–98%	[52]
Geometric control/chelation (bis-NHC Pd, Ru–NHC coumarin)	Bidentate or rigid scaffolds enhance stability and kinetics vs. mono-NHCs	η_{10} = 175 mV (Ru–NHC); η_{10} = 347 mV (bis-NHC Pd)	[45,48]
π-conjugated macrocycles/metallacycles (Ag_3L_3, Au_3L_3)	π–π stacking ensures electrode adhesion; conductivity is enhanced with carbon support	η_{10} = 187–416 mV (Ag_3L_3/C, Au_3L_3/C)	[51]
Hybrid nanostructures (MWCNT–NHC–Pt, NHC–$Cu_{3-x}P$)	NHCs stabilize ultrasmall NPs, modulate charge, and resist aggregation	See above; stable current over 6–24 h	[43,53]

3.2.1. Ligand-Centered vs. Metal-Centered H Binding as an Open Mechanistic Frontier

A recurring mechanistic debate in NHC-based HER catalysis is whether H–H bond formation comes from ligand-centered protonation or traditional metal–hydride pathways. In Ag and Au coumarin–NHC complexes, both experimental data and DFT calculations indicate that the NHC ligand itself functions as the proton-accepting site, with H binding occurring on the carbene framework instead of the metal. Conversely, Ni–amidate and Co–NHCU catalysts go through stepwise metal reduction and protonation to form distinct Ni–H or Co–H intermediates, aligning with standard HER mechanisms. This contrast raises a critical unresolved question: are ligand-centered pathways only feasible in noble-metal or weakly bound systems, or can they play a broader role in base-metal HER catalysts? Resolving this is essential, as it will determine whether NHCs should mainly be designed as proton relays or as scaffolds that stabilize the metal in HER catalysis.

3.2.2. Overall Concluding Remarks

Taken together, the studies above show that while NHC-based HER catalysis is still emerging, several consistent design principles can already be identified:

(1) Stabilization of metal(0) states under reductive bias. A unifying strength of NHC ligation is its ability to maintain metals in the zero oxidation state—the critical active form for HER. This is seen across molecular Ni(II)/Ni(I)/Ni(0) cycles, nanoscale $Cu_{3-x}P$, and especially in MWCNT–NHC–Pt hybrids, where NHC anchoring preserves Pt^0 sites and yields ultrahigh per-atom activity. This behavior distinguishes HER from CO_2RR, where higher oxidation states are often more relevant.

(2) Ligand vs. metal-centered reactivity. Coumarin–NHC Ag/Au systems show ligand-centered H binding, while Ni–amidate and Co–NHCU catalysts operate via metal–hydrides. Balancing these pathways remains an unresolved mechanistic frontier.

(3) Proton relays and biomimetic motifs. Pendant pyridinone or uracil groups act as intramolecular proton shuttles, enabling hydrogenase-like PCET and delivering some of the highest TOFs reported for base-metal HER systems.

(4) Geometric enforcement and chelation. Bis-NHC scaffolds and rigid architectures (Pd, Ru) improve stability and electron transfer efficiency versus monodentate systems.

(5) Macrocycles and metallacycles. π-conjugated NHC frameworks provide adhesion, conductivity, and durability on electrode surfaces, especially when combined with carbon supports.

(6) Hybrid nanostructures. NHC–metal interfaces stabilize ultrasmall nanoparticles, modulate surface charge, and resist deactivation, enabling HER activity with minimal noble-metal loading.

Looking forward, NHC ligands stand out for their unique ability to combine M^0 stabilization, enzyme-like proton relays, structural rigidity, and hybrid-material integration. This versatility positions them as powerful tools for advancing both base-metal and low-loading noble-metal HER catalysts, with implications for bifunctional water splitting and scalable hydrogen production.

4. Oxygen Evolution Reaction (OER)

While NHC-based electrocatalysis has been more extensively explored in CO_2RR and HER systems, recent advances have begun to demonstrate their potential in addressing the greater kinetic and thermodynamic demands of the oxygen evolution reaction (OER). The high overpotentials and oxidative conditions required for OER pose a significant challenge to ligand stability—making the strong σ-donor and redox-tunable properties of NHCs particularly attractive. Emerging studies now highlight how NHC coordination can stabilize high-valent metal centers, improve charge-transfer properties, and promote long-term activity. These contributions span molecular complexes, nanohybrids, and composite materials, including systems based on iridium and earth-abundant transition metals supported on conductive carbons.

4.1. NHC-Metal-Based OER Electrocatalysts

One of the first systems utilizing NHC ligands explored for OER involved a homogeneous Ni(II) complex bearing a macrocyclic NHC/pyridine hybrid ligand, which was evaluated for water oxidation in neutral and alkaline aqueous media [54]. This air- and moisture-stable molecular catalyst, NiL_2 (L = bis(2-pyridyl-methylimidazolylidene)methane), exhibited sustained catalytic activity at an overpotential of 0.80 V (GCE: ~0.55 V), reaching a stable current density of 0.65 mA cm^{-2} with 93% Faradaic efficiency during 11 h of bulk electrolysis. Extensive post-catalysis analyses (CV, UV-Vis, HR ESI-MS, SEM, EDX) confirmed the retention of the molecular structure, ruling out NiO_x formation. Interestingly, the catalytic performance in phosphate buffer was significantly enhanced compared to acetate at identical pH, supporting a proton-coupled electron transfer (PCET) mechanism facilitated by phosphate ions as proton acceptors. This study represents the first homogeneous Ni–NHC catalyst for water oxidation and emphasizes the combined impact of ligand design and electrolyte identity on molecular OER activity.

In parallel, Ir(I) complexes covalently anchored onto thermally reduced graphene oxide (TRGO) were developed by Jimenez and co-workers, as OER electrocatalysts, exploiting the residual hydroxyl groups of the carbon support for stable immobilization of Ir–NHC species [55]. Two types of TRGO supports, differing in domain size and distribution of sp^2/sp^3 regions, were employed to study the influence of carbon surface chemistry on catalytic behavior. The spatial proximity of sp^2 and sp^3 domains significantly affected the coordination environment of the iridium centers—particularly the retention or displacement of chlorido ligands—ultimately modulating the electrocatalytic performance. While the overall OER activity remained poor despite the use of a noble metal (η_{10} = 1150/1300 mV, Tafel slopes of 186/337 mV/dec), an intriguing observation was that catalysts

with preserved chlorido coordination exhibited markedly enhanced activity toward the OER. This underscores the importance of both the metal–ligand microenvironment and the electronic/structural properties of the carbon support in dictating electrocatalytic outcomes. The same group also reported further work by anchoring Ir–NHC complexes onto graphene oxide (GO) derived from industrial coke waste, highlighting a sustainable approach to support design [56]. Two synthetic strategies—direct graphene electrografting of the previously synthesized aniline-functionalized [IrI(cod)(4-$NH_2(C_6H_4)$ImMe] complex, and a two-step sequence comprising initial electrografting of aniline-imidazolium salts and subsequent chemical reaction with Ir(I) precursor [Ir(μ-OMe)(cod)]$_2$, anchoring the final Ir(I) molecular complex as in the previous strategy—were compared, with the latter offering superior activity and stability. The best activity, even though it's significantly low, was shown when GO from coke waste was used as a support for grafting the Ir (I) complex in a 2-step chemical reaction. Nevertheless, structural studies (XANES/EXAFS) confirmed that, even after catalysis, the iridium centers retained their square-planar coordination and molecular nature.

Another work was published in 2022 by Budagumpi and co-workers with the first report of NHC–gold(I) binuclear complexes as OER electrocatalysts [57]. Pyridine-functionalized NHC binuclear gold(I) metallacycles were prepared via Ag–NHC transmetallation. Structural analysis (X-ray) confirmed linear Au–C(carbene) and Au–N(pyridine) coordination with intramolecular Au-Au interactions (3.25 Å). When supported on conductive graphitic mesoporous carbon (10 wt%), these complexes achieved overpotentials of 1.192 and 1.140 V vs. RHE to reach 10 mA cm^{-2} in alkaline media, with Tafel slopes of 40.9 and 30.4 mV dec^{-1}, respectively. The catalysts also demonstrated electrochemical stability over repeated cycling, with the second complex presenting only minimal ~39 mV overpotential loss after 300 successive cycles. This study introduced gold-based NHC molecular electrocatalysts into the OER field, highlighting the role of bidentate ligand design and conductive supports, even though these results were again very poor.

2024 represents a turning point in the application of NHC ligands toward OER, with impressive independent studies demonstrating the feasibility of both molecular and hybrid NHC-based electrocatalysts under the demanding oxidative conditions needed for this reaction.

Budagumpi extended the work beyond noble metals, where Ni and Co NHC complexes with π-conjugated coumarin-based ligands were evaluated both as molecular electrocatalysts and in carbon composite forms for OER in alkaline media (1 M KOH) [58]. The carbon composites showed significantly enhanced performance compared to their parent complexes, achieving low overpotentials down to 323 mV at 50 mA cm^{-2} for the Ni(II) system (Table 5, entries 1 and 2) and reaching 100 mA cm^{-2} at overpotentials as low as 409 mV for the Co (III) system (Table 5, entries 3 and 4). These improvements were accompanied by excellent kinetics, with Tafel slopes reduced to 40 and 56 mV dec^{-1}, respectively—indicative of a shift in the rate-determining step at lower η relative to the molecular precursors. Chronoamperometric and chronopotentiometric measurements demonstrated high operational durability, with Ni (II)@graphene composite maintaining ~96% of its initial current density after 3.5 h at η_{10}. Electrochemical impedance spectroscopy (EIS) revealed lower charge transfer resistance (Rct) in the composites (15.10–17.47 Ω) versus the parent complexes (15.57–20.74 Ω), with the Ni (II)@graphene composite again outperforming in terms of both Rct and solution resistance (Rs). This performance was attributed to enhanced π–π stacking between the coumarin ligands and graphitic carbon, promoting improved charge transfer across the electrode interface. Mechanistically, strong NHC–M–OH interactions were identified as central to catalytic activity, while the conductive support amplified overall efficiency through facilitated electron transport. Collectively, this study showcased—*for the first time*—the full electrocatalytic potential of NHC-based architectures in OER using base metals, establishing a robust interface between ligand-directed molecular control and nanoscale materials engineering.

A significant advance was achieved in the recent work by Rapakousiou and co-workers, who reported a highly active and durable OER electrocatalyst based on NHC-ligated Ni nanoclusters (NiNCs) covalently anchored on MWCNTs (Figure 6a) [12]. The hybrid material was synthesized via in situ reduction of Ni(II) precursors in the presence of NHC ligands and MWCNTs, where transmetallation from Cu(I)–NHC to Ni(0) occurred under $NaBH_4$ reduction in aqueous conditions, leading to the formation of ultrasmall NiNCs (<1.6 nm) uniformly distributed on the carbon scaffold. Structural characterization via HRTEM, HAADF-STEM, and EDS mapping confirmed the efficient decoration of crystalline NiO/Ni(0) nanoclusters on the MWCNT surface, with NHC coordination stabilizing the metallic core and permitting surface shell oxidation to Ni(II) phases. In 1 M KOH, the MWCNT–NHC–NiNCs exhibited very low overpotentials of 320 mV at 10 mA cm^{-2} and 500 mV at industrially-relevant high current density of j = 200 mA cm^{-2}, and record-high specific and intrinsic activities of j_{ESCA}= 133 mA cm^{-2} and j_{nNi} = 2.8 × 10^9 mA mol^{-1}·cm^{-2}, respectively, outperforming state-of-the-art RuO_2 and advanced NiFe-based references (Table 5, entry 5). The electrocatalyst's architecture integrates a conductive NHC–Ni(0) core with an electroactive NiO_x shell, covalently anchored onto a mechanically robust and conductive MWCNT scaffold. The

Ni(0) core remained stable (not oxidized) due to strong NHC ligation, while the NiO_x shell—confirmed by CV to undergo dynamic oxidation just prior to OER onset—enabled redox flexibility across all OER steps, allowing for surface restructuring and stabilization into a highly uniform electroactive state. This is further supported by the low Tafel slope of 51 mV dec^{-1}, indicative of a rate-determining step (RDS) involving the oxidation of adsorbed hydroxide species (OH*) to oxygen intermediates (O*), characteristic of efficient OER catalysts. Electrochemical impedance spectroscopy (EIS) revealed a progressive drop in charge transfer resistance (Rct) from 66 to 9.7 Ω with increasing overpotential, reflecting improved interfacial electron transport and robust kinetics. Notably, sharp transitions in Rct slope around 2.5 and 7 mA cm^{-2} pointed to distinct changes in the RDS—from Ni(II) oxidation to oxygen evolution—under increasingly oxidative conditions. Long-term potentiometry and cycling further demonstrated outstanding durability, with <1.3% overpotential gain after 10,000 successive cycles. The covalently engineered nanoarchitecture ensures near-complete utilization of Ni active sites and excellent resistance to oxidative degradation under industrially relevant OER conditions.

Table 5. NHC-based efficient electrocatalysts for OER.

	NHC-Metal System	Conditions	η (mV)	Tafel Slope (mV/dec)	Rct (Ω)	Ref.
1	**Ni (II)–NHC–benzo [7,8]coumarin/ @graphene composite**	1 M KOH, Glassy carbon RRDE	η_{50} = 373/323	89/40	~18/~16	[58]
2	**Ni (II)–NHC–benzo [5,6]coumarin/ @graphene composite**	1 M KOH, Glassy carbon RRDE	η_{50} = 389/330	98/46	~18/~16	[58]
3	**Co (III)–NHC–benzo [7,8]coumarin/ @graphene composite**	1 M KOH, Glassy carbon RRDE	η_{50} = 415/348	100/56	~18/~16	[58]
4	**Co (III)–NHC–benzo [5,6]coumarin/ @graphene composite**	1 M KOH, Glassy carbon RRDE	η_{50} = 424/373	122/70	~18/~16	[58]
5	**MWCNTs-NHC-Ni(0)NiO_x nanoclusters**	1 M KOH, Glassy carbon	η_{10} =320	51	45 ($j_{2.5\ mA/cm2}$) and 12 ($j_{10\ mA/cm2}$)	12

A final example involves a Pd–NHC nanoparticle catalyst supported on plastic-derived carbon (PdNPs@PC–NHC), deposited on Ni foam and evaluated for OER in 1 M KOH electrolyte under standard three-electrode conditions [59]. While the catalyst achieved an overpotential of 310 mV at 40 mA cm^{-2} and a Tafel slope of 46 mV dec^{-1}, the improvement over bare Ni foam and carbon support was modest. EIS confirmed reduced charge transfer resistance (Rct = 12 Ω), and 24 h chronoamperometry demonstrated good stability. However, the work primarily represents a functionalization of an existing Ni foam-based platform rather than a significant advance in OER performance. Still, the use of waste-derived PET carbon aligns with sustainability goals, and the study demonstrates that NHC ligands can be integrated into low-cost, scalable architectures.

4.2. Concluding Remarks on OER

To synthesize the various studies discussed above, Table 6 summarizes the key structural motifs of NHC–metal OER electrocatalysts, linking each design element to its mechanistic role and typical performance benchmarks. This framework highlights how NHC ligation can stabilize high-valent states, facilitate charge transfer, and improve durability under demanding anodic conditions—while also emphasizing the ongoing debate about their oxidative stability.

Table 6. Structural–performance correlations in NHC–metal OER electrocatalysts.

Structural Motif/Design Strategy	Mechanistic Consequence	Performance Anchor	Ref.
Macrocyclic Ni–NHC–pyridine complexes	Stabilize Ni(II) centers, prevent NiO_x formation; PCET facilitated by phosphate buffer	$\eta \approx 0.80$ V, FE 93%, stable 11 h	[54]
Ir–NHC on graphene/TRGO supports	Support chemistry (sp^2/sp^3, chloride retention) alters Ir coordination; dictates activity	η_{10} = 1150–1300 mV, Tafel 186–337 mV/dec (poor OER)	[55,56]
Binuclear Au(I)–NHC metallacycles (pyridyl-NHC)	Au–Au interactions; conductive carbon support critical	η_{10} = 1140–1192 mV, Tafel ~30–40 mV/dec; stable after 300 cycles	[57]

Table 6. *Cont.*

Structural Motif/Design Strategy	Mechanistic Consequence	Performance Anchor	Ref.
Coumarin–NHC Ni/Co complexes → carbon composites	π–π stacking with graphene enhances charge transfer, lowers Rct; strong NHC–M–OH interactions enable OER	η_{10} = 323–348 mV, Tafel 40–56 mV/dec; sustained 3.5 h	[58]
MWCNT–NHC–Ni nanoclusters (Ni^0 core/NiO_x shell)	NHC stabilizes Ni^0 core; dynamic NiO_x shell provides redox flexibility; covalent anchoring ensures durability	η_{10} = 320 mV; η_{200} = 500 mV; Tafel 51 mV/dec; <1.3% loss after 10,000 cycles	[12]
Pd–NHC NPs on waste-derived carbon	Sustainable carbon support; modest enhancement; stable 24 h	$\eta_{10} \approx 310$ mV at 40 mA cm^{-2}; Tafel 46 mV/dec	[59]

4.2.1. Oxidative Stability at High Anodic Potentials

This focus on hybrid design highlights the exceptional oxidative stability needed for OER, which usually occurs at anodic potentials above 1.5 V vs. RHE. An ongoing debate in the field is whether NHCs are inherently stable at such oxidizing potentials or if stability only occurs when NHCs are incorporated into protective hybrid structures. For instance, surface-enhanced Raman spectroscopy (SERS) studies reveal that simple NHC monolayers on gold degrade beyond ±1 V vs. Ag/AgCl during extended electrochemical cycling, and minor backbone modifications considerably change their electrochemical lifetimes. In contrast, the covalently engineered NHC–Ni nanocluster system mentioned earlier showed almost no activity loss after 10,000 continuous cycles, emphasizing that covalent immobilization and electronic shielding—not just the carbene itself—are key for long-term operation under OER conditions.

4.2.2. Overall Concluding Remarks

The diverse examples surveyed here establish that NHC-based architectures form a robust and modular platform for OER. Whether integrated into molecular complexes, hybrid nanocomposites, or nanoparticle–carbon hybrids, NHC ligands offer a combination of electronic tunability, robust metal–ligand binding, and anchoring versatility that is well suited to the harsh oxidative demands of the OER.

Notably, the highest OER performances were achieved by hybrid constructs integrating NHC–metal active sites with conductive carbon scaffolds—an approach that drastically improves both activity and durability. Through such designs, base-metal NHC catalysts developed in 2024–2025 have reached overpotentials in the range of 320–350 mV (at 10–50 mA cm^{-2}) and sustained current densities up to 100–200 mA cm^{-2} at <0.5 V overpotential [12,58]. These figures rival or even surpass traditional benchmarks like NiFe oxyhydroxides and RuO_2, highlighting a remarkable leap in performance. Achieving this required robust catalyst architectures: NHC ligation provides strong metal–ligand bonds and electronic adaptability, while conductive carbon supports ensure fast charge transport and mitigate degradation. This emphasis on hybrid design reflects the exceptional oxidative stability required for OER, which typically operates at anodic potentials above 1.5 V vs. RHE. In this regime, purely molecular or monolayer-based systems often degrade unless carefully stabilized. Indeed, surface-enhanced Raman spectroscopy (SERS) studies have shown that NHC monolayers on gold deteriorate beyond ±1 V vs. Ag/AgCl under prolonged electrochemical cycling, and that subtle modifications to the NHC backbone can significantly influence their electrochemical lifetime [7]. In stark contrast, the covalently engineered NHC–Ni nanocluster system discussed above exhibited nearly no activity loss after 10,000 continuous cycles, underscoring the advantages of covalent immobilization and electronic shielding.

Together, these studies reveal that NHCs are not merely passive ligands, but active contributors to charge transfer, catalyst stabilization, and dynamic interfacial electronic structure. As the field moves forward, this synergy of molecular design and materials engineering offers a unique molecular toolkit for constructing robust, scalable, and industrially viable OER electrocatalysts. The advances in OER-specific systems also lay a foundation for NHC-based catalysts in more complex or bifunctional water-splitting platforms, where both hydrogen and oxygen evolution must be efficiently coordinated—as explored in the following section.

5. Water-Splitting

5.1. NHC–Metal-Based Bifunctional Electrocatalysts for Overall Water Splitting

Budagumpi and co-workers have recently introduced a series of bifunctional NHC–metal electrocatalysts capable of driving both HER and OER in alkaline media. By employing strategic integration with carbon-based

supports—including carbon cloth, graphene, and carbon nanotubes—they demonstrated enhanced overall water-splitting performance through both molecular and composite catalyst architectures.

In one such example, the non-covalent immobilization of NHC–metal complexes onto carbon cloth (CC) enabled the fabrication of free-standing bifunctional electrodes for overall water splitting [60]. Complexes of Co, Ni, and Pd bearing a pyridine-functionalized NHC ligand (HLBr) were synthesized and dip-coated onto CC, allowing direct HER and OER testing in 1 M KOH (Figure 6b). Among them, $CoLBr_2$@CC exhibited the best HER activity (η_{10} = 256 mV, Tafel slope = 155 mV dec^{-1}), while $NiLBr_2$@CC showed the highest OER performance (η_{10} = 376 mV, Tafel slope = 86 mV dec^{-1}). These bifunctional electrodes were successfully used to assemble a symmetric alkaline electrolyzer ($CoLBr_2$//$CoLBr_2$) that operated—as the authors claim—at 1.81 V to achieve 10 mA cm^{-2}. This value appears significantly lower than expected based on the individual HER and OER overpotentials (η_{10} = 256 and 444 mV, respectively), suggesting possible inconsistencies in data extraction, reporting, or cell configuration. Post-electrolysis characterization (XPS, IR, SEM) confirmed excellent chemical robustness, with minimal leaching and no detectable structural degradation. This study demonstrates that even simple, non-covalent immobilization approaches can produce molecularly-defined NHC-based electrocatalysts that are highly effective for integrated HER and OER under alkaline conditions.

A related carbon composite strategy was employed to enhance the bifunctional electrocatalytic performance of metal–NHC complexes by integrating them with multiwalled carbon nanotubes (MWCNTs) or graphene plates (GP), enabling overall water splitting in both acidic and alkaline media (Figure 6c) [61]. Complexes of Pd, Ni, and Co were prepared and characterized, and their HER and OER activities were systematically evaluated. While the pristine complexes showed moderate activity (HER η_{10} = 655 to 775 mV; OER η_{10} = 324–372 mV), incorporation into conductive carbon scaffolds significantly boosted performance. The Pd-NHC-based composite@MWCNT emerged as the most active HER electrocatalyst (η_{10} = 440 mV in 0.5 M H_2SO_4), while the Ni-NHC-based@MWCNT composite demonstrated excellent OER activity (η_{10} = 229 mV in 1 M KOH), outperforming its molecular precursor. Tafel slope analyses and electrochemical impedance spectroscopy confirmed enhanced charge transfer kinetics and reduced resistance at the electrode–electrolyte interface. Moderate chronoamperometric stability was observed (5 h), attributed to the protective effect of the NHC and pyridyl ligands. This study reinforces the value of modular NHC–metal frameworks and carbon hybridization for designing earth-abundant, bifunctional electrocatalysts for water splitting.

A complementary strategy employed non-covalent π–π stacking to fabricate bifunctional Ni–NHC–MWCNT composite electrodes (Figure 6d) [62]. The Ni(II)–NHC complex, derived from a π-conjugated coumarin-functionalized carbene ligand, was integrated with multiwalled carbon nanotubes (MWCNTs) in varying ratios (100:0 to 80:20 wt%) to yield a series of composite materials. Among them, the 90:10 wt% composite delivered optimal electrocatalytic performance. For the OER in 1 M KOH, it exhibited a low overpotential of 380 mV at 10 mA cm^{-2} with a favorable Tafel slope of 114 mV dec^{-1}, outperforming the bare complex (η_{10} = 434 mV, Tafel slope = 93 mV dec^{-1}). EIS studies confirmed that this composite presented very fast charge transfer kinetics with a Rct = 8 Ω. In the HER, it also showed improved activity in 0.5 M H_2SO_4 with an overpotential of 364 mV and a reduced Tafel slope of 51 mV dec^{-1}, compared to 412 mV and 139 mV dec^{-1} for the unmodified complex. Electrochemical impedance spectroscopy confirmed that this composite had the lowest charge transfer resistance in 0.5 M H_2SO_4 (Rct = ~100 Ω, assumed), along with a higher double-layer capacitance (Cdl = 8.2 mF cm^{-2}), indicating improved active site accessibility and enhanced charge transport. These enhancements were attributed to strong π–π stacking interactions between the coumarin ligand and MWCNT walls, which not only stabilized the Ni–NHC interface but also facilitated efficient electron mobility across the composite matrix. Moderate durability was also demonstrated through 2000 continuous LSV cycles with ~ 10% performance loss. Overall, this study showcases how π-conjugated NHC ligands can be rationally paired with conductive nanocarbon supports to engineer bifunctional, durable, and high-performing electrocatalysts for water splitting.

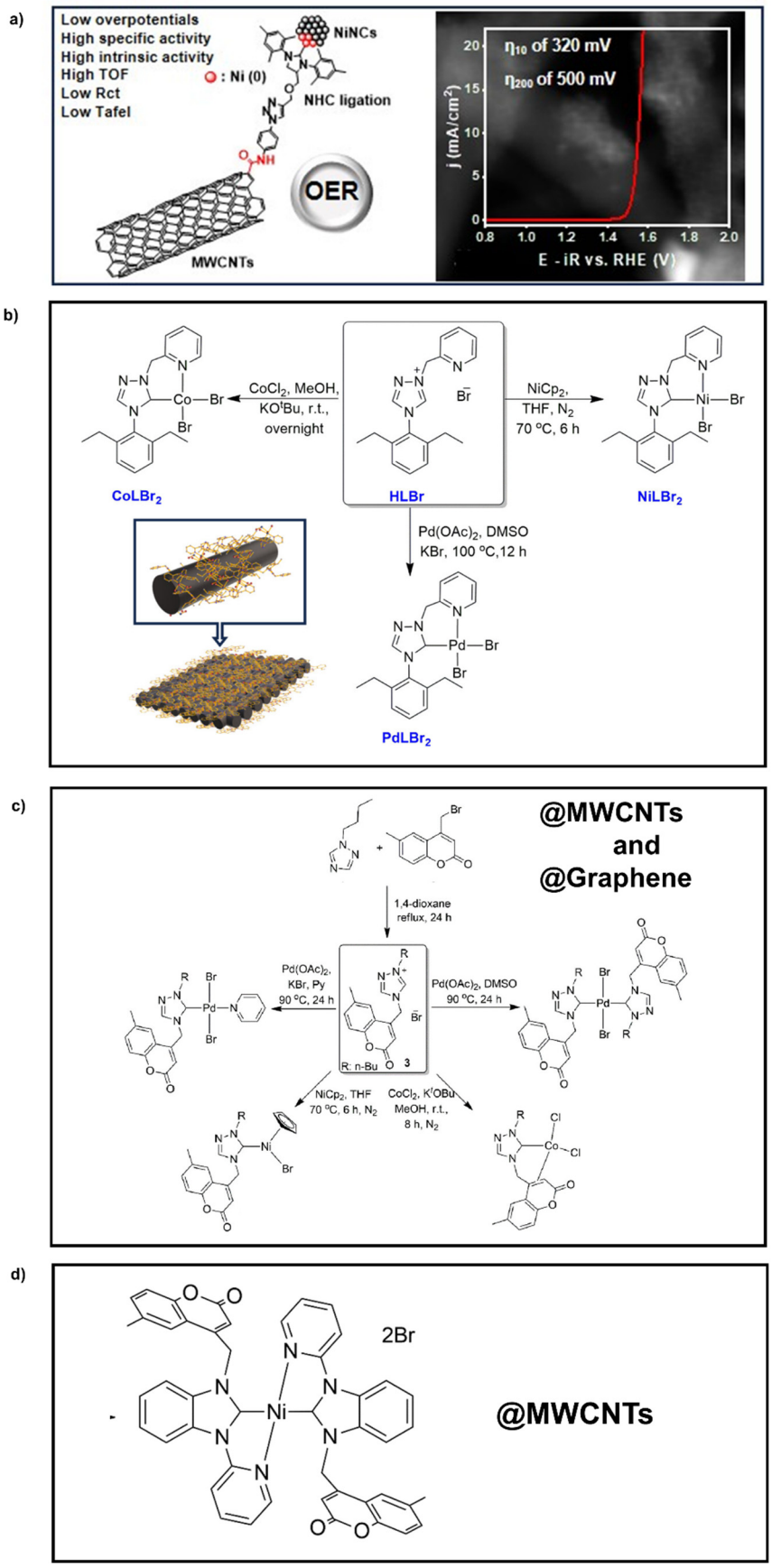

Figure 6. NHC-based electrocatalysts for OER (Water Oxidation) and overall Water-Splitting: (**a**) MWCNTs-NHC-Ni(0)NiO_x platform for efficient electrocatalysis surpassing NiFe systems and RuO_2. Reproduced from Ref. 12 with permission from the Royal Society of Chemistry, (**b**) $CoLBr_2$, $NiLBr_2$, and $PdLBr_2$ complexes non-covalently immobilized on carbon cloth via dip-coating, forming molecularly modified free-standing electrodes. Adapted from Ref. [60] with permission from the American Chemical Society, (**c**) Pd, Ni, and Co–NHC complexes supported on MWCNTs or graphene plates, yielding composite bifunctional electrocatalysts for HER and OER.

The carbon nanocomposites significantly enhanced activity and charge transfer kinetics. Adapted from Ref. [61] with permission from the American Chemical Society, (**d**) Nickel(II)–NHC complex bearing a coumarin-functionalized ligand integrated with MWCNTs via non-covalent π–π stacking to form composite bifunctional electrocatalysts. Adapted from Ref. [62] with permission from the American Chemical Society.

5.2. Early Concluding Remarks on Water-Splitting

In summary, the bifunctional NHC–metal systems presented here reveal clear design trends for advancing overall water splitting. Since the oxygen evolution reaction (OER) remains the primary kinetic bottleneck in alkaline electrolysis, the most effective systems are those in which NHC–metal centers are integrated into conductive carbon nanostructures—such as carbon cloth, graphene, or MWCNTs. These architectures enhance charge transport and stabilize the catalyst interface under harsh oxidative conditions. Durability, however, is not merely a desirable feature but a critical priority for water-splitting technologies. The highest OER durability and current densities are achieved through nanocomposite or covalent hybrid designs that provide molecular-level control over catalyst architecture—such as covalently anchored NHC–metal nanostructures.

Notably, while several base metals have been explored, only redox-adaptive systems—such as those based on cobalt and, to a lesser extent, nickel—consistently deliver strong performance across both HER and OER. This likely stems from their ability to access and stabilize both high and low oxidation states. These observations underscore the dual importance of judicious metal selection and intelligent ligand integration via precise nanoengineering. The exploration of NHC–metal platforms for water splitting is still in its early stages—and with the ongoing convergence of ligand design and materials engineering, more advanced and durable systems are poised to follow.

An unresolved question is whether molecular NHC–metal complexes can resist the oxidative bias of OER on their own or if hybridization with conductive carbon frameworks is always necessary. So far, only hybrid or composite designs achieve industrially relevant durability, indicating that integration with conductive support may be essential. Tackling this stability issue will be crucial for advancing NHC–metal catalysts beyond early proof-of-concept water-splitting systems.

6. Other Emerging NHC-Based Electrocatalytic Transformations

While most NHC-based electrocatalysis has centered on CO_2 reduction, followed by HER and, more recently, limited studies on water oxidation, several emerging efforts have extended NHC applications to broader electrochemical transformations—including oxygen reduction (ORR), ammonia oxidation, and urea electrosynthesis. These exploratory studies highlight the expanding versatility of NHC ligands across diverse redox environments and reaction pathways.

Beyond OER, in the earlier discussed work from 2024, the Ni(II)–NHC@graphene composite also exhibited efficient electrocatalytic activity toward the oxygen reduction reaction (ORR) in alkaline media (Figure 5e) [58]. The same π-conjugated NHC ligand and conductive carbon synergy that enhanced its water oxidation performance also facilitated selective two-electron ORR to hydrogen peroxide (H_2O_2) in 1 M KOH. Under RRDE conditions at 2000 rpm, the nanocomposite delivered an overpotential of just 323 mV vs. RHE, with a disk current density of 50 mA cm^{-2}, and a simultaneous ring current of 0.6 mA cm^{-2} was detected at the Pt ring electrode held at 1.8 V, confirming high selectivity for H_2O_2 production. At elevated potentials, the disk current further increased to 150 mA cm^{-2}, indicating robust catalytic activity over a wide potential window. The onset potential was close to the thermodynamic limit for the two-electron pathway, consistent with an outer-sphere electron transfer mechanism involving solvated O_2 and surface hydroxyl species. This selective peroxide generation—combined with the composite's low charge transfer resistance, good electrochemical stability, and synergistic nanoarchitecture—demonstrates the broader promising potential of NHC–metal composites for dual-function electrocatalytic platforms, including sustainable H_2O_2 electrosynthesis.

A rare example of molecular electrocatalytic ammonia oxidation using NHC ligands was recently demonstrated with the iron(II) complex trans-$[LFe(MeCN)_2]^{2+}$, where *L* is a macrocyclic tetracarbene ligand comprising four N-heterocyclic carbene donors (Figure 7a) [63]. This Fe complex catalyzed the oxidation of NH_3 to N_2 in both chemical and electrocatalytic regimes with high efficiency and remarkably low catalyst loading (0.043 mM, 0.004 mol% catalyst). Under chemical conditions at –30 °C and using the triarylaminium oxidant $[(p\text{-}MeOC_6H_4)_3N]^+$, the system achieved up to 182 turnovers of N_2, marking the highest reported value for a soluble molecular catalyst to date. This reactivity was successfully translated into mediated electrocatalysis, employing the same organic oxidant as a redox mediator. At –20 °C, the system exhibited an onset potential of 0.09 V and Ecat/2 of 0.18 V vs. $Fc^+/0$, delivering 9.3 TONs of N_2 with 75% Faradaic efficiency. The mediator not only

facilitates heterogeneous electron transfer at the electrode interface but also assists in PCET at the Fe center, particularly at axial N_xH_y moieties. DFT calculations suggest a mechanistic pathway involving oxidation and deprotonation of coordinated NH_3 to form a $[LFe^{IV}(NH_2)_2]^{2+}$ intermediate, followed by bimetallic N–N coupling to generate hydrazido species en route to N_2 evolution. The rigid tetra-NHC macrocycle plays a crucial role in stabilizing high-valent Fe intermediates and suppressing ligand dissociation, a common deactivation pathway in NH_3 oxidation. Altogether, this study illustrates how combining robust carbene coordination with redox-mediating strategies can unlock challenging transformations in nitrogen activation and offers a promising template for advancing ammonia-based energy conversion.

NHC ligands have also been integrated into atomically precise alloy nanoclusters for the tandem electrosynthesis of urea from CO_2 and nitrate [64]. A recent study reported the synthesis of a rod-like $Au_{13}Ag_{12}$ nanocluster ligated by two benzimidazolium-derived NHCs (BMIm), along with phosphine and iodide co-ligands, yielding the alloy $[Au_{13}Ag_{12}(PPh_3)_8(BMIm)_2I_8]^+$ (Figure 7b). Anchored on NiFe layered double hydroxide (NiFe-LDH) supports, this nanocluster catalyzed the electrochemical coupling of nitrate and CO_2 to urea with a Faradaic efficiency of 34% and a production rate of 29.5 mmol g_{cat}^{-1} h^{-1} at –0.5 V vs. RHE, outperforming its phosphine-only analogue. The bimetallic core adopts a vertex-sharing biicosahedral structure, with DFT calculations revealing significant frontier-orbital delocalization across the Au–C_NHC interface. This strong Au–carbene bonding not only enhances electronic communication and charge delocalization but also imparts superior thermal stability and light sensitivity to the nanocluster. Mechanistically, the system leverages the synergistic interface between AuAg nanoclusters and NiFe-LDH, where *CO and *NH_2 intermediates—formed via CO_2 and NO_3^- reduction, respectively—undergo C–N coupling to yield urea. This study marks a significant advance in NHC-ligated nanocluster chemistry, demonstrating how NHCs can stabilize alloyed active sites for dual-substrate electrosynthetic transformations, and opening new avenues for designing tandem catalysis platforms targeting value-added nitrogen-containing products.

Together, these studies demonstrate that NHC ligands extend well beyond classic electrocatalytic frameworks, enabling selective and efficient transformations in less conventional but increasingly important areas of energy and environmental catalysis. Their unique electronic effects, binding strength, and structural versatility offer continued promise for the rational development of next-generation catalysts across a broader reaction landscape.

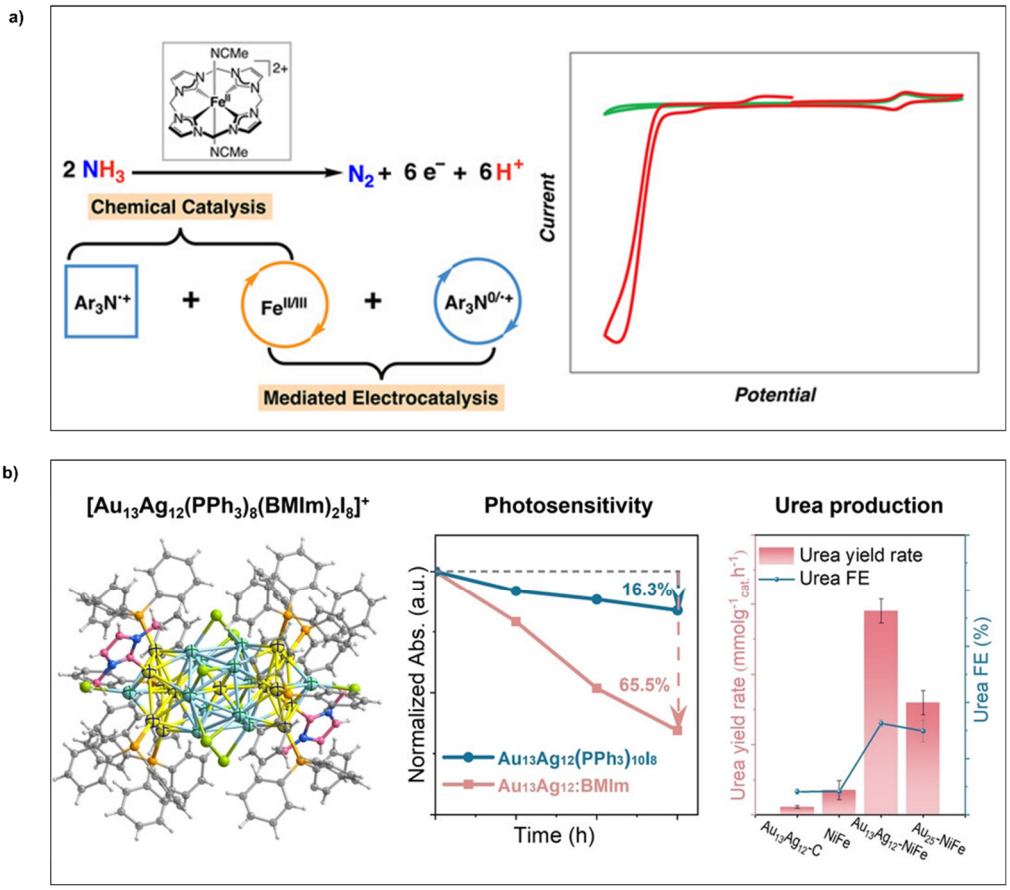

Figure 7. Other NHC-based electrochemical transformations: (**a**) electrocatalytic oxidation of ammonia to N_2 mediated by a macrocyclic Fe(II) trans-$[LFe(MeCN)_2]^{2+}$complex bearing four NHC donors and a triarylaminium

redox mediator; the system achieves high FE (75%). Reproduced from Ref. [63] with permission from the Wiley-VCH GmbH, (**b**) electrosynthesis of urea from the co-reduction of nitrate and CO_2 using atomically precise $[Au_{13}Ag_{12}(PPh_3)_8(BMIm)_2I_8]^+$ nanoclusters stabilized by benzimidazolium NHC ligands (BMIm) and supported on NiFe layered double hydroxide (LDH); achieving 34% FE. Reproduced from Ref. [64] with permission from the Wiley-VCH GmbH.

7. Conclusions and Outlook

NHC ligands have emerged as powerful modulators of electrocatalytic reactions across multiple scales, from discrete molecular complexes to nanoclusters and surface-bound assemblies. By their strong σ-donor and π-acceptor character, NHCs finely tune the metal–ligand electronic structure, shifting metal redox potentials and adjusting the binding of key intermediates. These effects translate into broad performance gains: NHC coordination can pre-activate substrates and optimize proton/electron-transfer steps, elevating the activity of multi-electron catalysts in CO_2 reduction, water splitting (HER/OER), and beyond. Mechanistic studies underline this impact. *On catalyst surfaces*, NHC adlayers directly modify adsorption energetics; for example, on Cu electrodes, NHC binding strengthens the Cu–CO interaction and cuts the *CO hydrogenation barrier by more than half, even turning a subsequent CO–CHO coupling step from endothermic to exothermic. In molecular complexes, carefully designed Ni(II) macrocyclic catalysts featuring redox-active NHC scaffolds show coupled metal–ligand redox behavior that biases the reaction pathway toward CO_2 reduction over competing proton reduction [65]. At the nanoscale, NHC-stabilized Pt nanoclusters on carbon supports exhibit a reversible Pt^0/Pt^{2+} redox cycle under HER conditions, indicating that the carbene–metal interface can adapt oxidation state to stabilize proton-reduction intermediates. In all these contexts, NHC ligation rigidifies the metal site's geometry and electronic environment in a way that boosts catalytic kinetics and selectivity.

NHCs also excel at bridging homogeneous and heterogeneous catalysis by enabling atomically dispersed yet robust active sites on electrode surfaces. The combination of nanoscale structuring with covalent NHC anchoring has proven key to maximizing catalyst utilization and longevity. Precisely tethering NHC–metal centers onto conductive scaffolds (carbon nanotubes, graphitic electrodes, etc.) yields catalysts with near-100% metal dispersity and exceptionally strong metal–support bonding. For instance, NHC-capped PtNPs (~2 nm) grown on MWCNTs deliver efficient hydrogen evolution (η_{10} = 77 mV at 10 mA·cm^{-2}, Tafel ~50 mV/dec) despite an ultralow 0.4% Pt atomic loading. Crucially, the NHC–metal bonding prevents Pt sintering or irreversible oxidation: even after prolonged cycling and air exposure, the NHC–Pt system maintains a stable, reversible Pt(0)/Pt(II) redox transition with negligible activity loss. Similarly, oxidized CNTs functionalized with NHC-bound Ni nanoclusters convert in situ into active NiO/NiOOH OER electrocatalysts, wherein essentially every Ni atom is electrochemically accessible. The robust Ni–C_{NHC} bond persists through the Ni(0)→Ni(III) transformation, so that NHC–Ni/MWCNT electrodes retain >99.5% of their Ni sites even after 10,000 OER cycles. In these examples, the covalent NHC anchoring provides strong mechanical support and efficient electron-transfer pathways, preventing nanoparticle coalescence and metal leaching. The result is dramatically enhanced durability compared to analogous non-NHC systems. (Notably, an NHC–Ni/MWCNT anode has outperformed even noble-metal benchmarks like RuO_2 in long-term OER stability, while an NHC–Pt/MWCNT cathode showed markedly suppressed Pt dissolution under sustained HER operation.)

Another defining virtue of NHC ligands is the redox flexibility they impart to catalytic sites. The strong σ-donation of NHCs stabilizes metals in unusually high or low oxidation states (e.g., Ni^{3+} in NiOOH or $Pt^{0/2+}$ in surface oxides). At the same time, the ligand's tunable π-system can engage in its reversible redox steps. In effect, NHC-ligated catalysts can "ride out" extreme potentials by redistributing charge between the metal center and the ligand. This adaptability is evident in operando: under anodic bias, an NHC–Pt^0/CNT catalyst will temporarily form a Pt^{II}–O (surface oxide) phase and then revert to Pt^0 upon returning to reducing conditions—effectively storing and releasing charge to facilitate proton reduction. In alkaline OER, an NHC-bound Ni catalyst likewise develops a NiOOH active layer without any loss of the NHC ligand; the strong Ni–C bond helps stabilize critical Ni–OH/O intermediates throughout the water-oxidation cycle. Thanks to this redox adaptability, NHC-modified catalysts tolerate highly oxidizing or reducing environments that would rapidly deactivate conventional complexes. They exhibit extraordinarily low metal dissolution and performance decay under harsh cycling. For example, the NHC–Ni/MWCNT system maintains its OER activity far longer than standard Ni or even precious-metal catalysts, and the NHC–Pt/CNT system shows only minimal Pt loss during extended HER electrolysis. By stabilizing reactive metal–oxo, metal–hydride, and *CO/*CO_2 adducts, NHC ligands not only boost catalytic turnover but also preserve the integrity of active sites under working conditions.

A significant advantage of NHC chemistry is its universality and tunability across different metals and material platforms. NHCs form strong bonds with a wide swath of the periodic table—from first-row transition metals (Fe, Co, Ni, Cu) to noble metals (Pd, Pt, Au) and even main-group elements—offering a unified design handle for diverse catalysts. This ligation strategy transcends the homogeneous/heterogeneous divide: NHCs have been employed as traditional ligands in molecular electrocatalysts (including *macrocyclic* Ni and Co complexes for water oxidation and CO_2 reduction), as self-assembled monolayers or adlayers on bulk metal electrodes (Au, Ag, Cu), and as surface-capping/stabilizing agents on colloidal metal nanoclusters (e.g., Pt, Pd, Au). In each context, the NHC's substituents can be tailored to tune steric bulk, donor strength, and electronic delocalization. For example, incorporating extended π-conjugated backbones or charged groups into an NHC allows electron density to delocalize into supporting carbon frameworks, as shown with π-extended NHCs on graphene that improve electronic conductivity. Likewise, polymeric NHC networks (such as the recently reported "ballbot"-type NHC monolayers on Au(111)) are opening up robust 2D architectures, essentially grafting a carpet of NHC active sites onto electrode surfaces. In essence, the same fundamental coordination chemistry and ligand design principles can be applied seamlessly in both molecular and heterogeneous settings. Across all platforms, we observe common NHC-induced benefits: enforcement of low-coordinate metal geometries, strengthened metal–support coupling, and an electron-buffering effect at the active site. This consistency underscores NHCs as a uniquely versatile ligand toolkit—essentially a molecular "Swiss army knife"—for bridging homogeneous and heterogeneous electrocatalysis.

Emerging NHC-Based Design Strategies: Building on these successes, researchers are developing next-generation NHC ligands and architectures to push catalytic performance even further:

(a) Macrocyclic NHCs: Rigid multidentate frameworks that incorporate multiple NHC donors into a cyclic ligand (analogous to porphyrins or other coordination macrocycles). These NHC macrocycles confer a preorganized geometry and often function as redox-active ligands, sharing electron density with the metal center to facilitate multi-electron processes. Such designs have shown enhanced stability and reactivity—for example, cobalt and iron complexes bearing NHC-containing macrocycles exhibit improved CO_2 reduction and ammonia oxidation performance under this cooperative metal–ligand redox behavior.

(b) Redox-Active NHCs: Tailoring the NHC scaffold itself to participate directly in redox chemistry. This can involve integrating conjugated aromatic backbones or redox-active pendants (e.g., viologen-, quinone-, or ferrocene-functionalized NHCs), enabling the ligand to accept or donate electrons reversibly. By acting as an internal electron reservoir, a redox-active NHC can buffer the oxidation state of the metal during catalysis, stabilizing high-energy intermediates and opening pathways to challenging multi-electron transformations (such as coupling CO_2 into C_2^+ products).

(c) Polymer-Anchored NHCs: Grafting NHC units onto polymer supports or into networked frameworks to create hybrid catalyst architectures. In these systems, NHCs are deployed in high density over a macroscopic substrate (e.g., a metallated polymer, metal–organic framework, or covalent organic layer on an electrode). This approach marries the tunability of molecular catalysts with the robustness and scalability of polymers, yielding electrode materials that maintain molecular-level control of active sites while significantly improving stability, conductivity, and ease of integration.

These emerging strategies highlight the rich design space now accessible with carbene ligands. By extending NHC coordination into macrocyclic, redox-active, and polymeric regimes, researchers are equipping catalysts with new ways to manage electrons and protons—a critical step toward overcoming current limitations in efficiency and selectivity.

Looking forward, realizing the full promise of NHC-based electrocatalysts will hinge on tightly integrating advanced characterization, theoretical insight, and clever ligand design. Operando characterization is especially vital: applying in situ spectroscopic probes (IR, Raman, XAS, etc.) under working electrochemical conditions can elucidate the fate of NHC-bound intermediates and active sites in real time. Such studies have already proven transformative in uncovering active phases and deactivation pathways in other catalyst systems and bringing the same tools to NHC–metal catalysts will clarify how key species (e.g., bound CO_2/CO adducts, metal–hydrides, or metal–oxo/hydroxides) form and evolve during catalysis [66]. Parallel computational efforts will complement the experiment by screening and refining new ligand constructs. For instance, ab initio modeling can evaluate how various NHC electronic modifications (electron-rich vs. electron-poor substituents, incorporation of redox-active backbones, addition of hydrogen-bond donors, etc.) influence reaction energetics. This approach can guide the design of NHC ligands that promote complex multi-step conversions—e.g., enabling cascade reduction of CO_2 beyond one-electron products or modulating proton-coupled electron transfer steps in HER. By identifying promising ligand candidates in silico, researchers can target synthetic efforts toward NHCs that will best stabilize intermediates and facilitate complicated bond-forming steps.

In this context, emerging machine learning (ML)-guided platforms may accelerate the exploration of vast NHC chemical space. Generative models and data-driven descriptor libraries tailored to NHC frameworks could facilitate inverse catalyst design, allowing for property-optimized NHC ligands to be suggested computationally before synthesis. Training such models on electrochemical data (e.g., TOF, η, FE) could reveal structure–function correlations and predict optimal combinations of NHC sterics, electronics, and backbones for different metal centers and reactions.

Equally important is the drive toward industrial integration of NHC-based catalysts. To meet practical requirements, these systems must operate efficiently at high current densities (hundreds of $mA \cdot cm^{-2}$) and maintain performance over prolonged operation. Achieving this will require innovation not just in molecular design but also in electrode engineering. One promising direction is the development of hierarchical 3D electrodes functionalized with NHC ligands. For example, a porous or nanostructured scaffold (such as a foam, aerogel, or interwoven carbon architecture) coated with NHC-bearing active sites could combine a large electrochemical surface area with excellent mass transport and robust ligand anchoring. Such an approach would ensure that even at high current loadings, reactants and electrolytes can access the NHC–metal sites, while the ligands remain securely attached to prevent catalyst degradation. An up-and-coming format is the zero-gap membrane electrode assembly (MEA), where the integration of NHC-modified catalysts with functionalized gas-diffusion layers (GDLs) could enhance mass transport and stabilize interfaces under high current, low-resistance operation. GDLs bearing covalently immobilized NHC–metal complexes may improve interfacial contact, water management, and long-term adhesion of the active layer. Throughout scaling-up efforts, continued operando monitoring will be indispensable to track structural and chemical changes under realistic conditions, allowing for iterative improvements in stability.

Nonetheless, several industrial hurdles remain. The cost and synthetic complexity of specific NHC ligands—especially those with bulky or redox-active frameworks—can pose a barrier to large-scale deployment. Efforts toward ligand streamlining, modular synthesis, and the use of sustainable carbene precursors (e.g., bio-derived imidazolium salts) will be essential to reduce costs. Similarly, colloidal nanocluster synthesis and surface functionalization processes must be adapted to scalable, reproducible routes that maintain control over ligand density and cluster size. Moreover, long-term stability of NHC–metal interfaces under MEA cycling conditions, including resistance to mechanical stress, flooding, or electrolyte degradation, will require focused study. Designing NHC-based materials that are compatible with commercial fabrication (e.g., inkjet printing, spray deposition) may help translate lab-scale innovations to device-level applications.

In parallel, exciting future directions include the design of NHC-based photoelectrodes and photoanodes for solar-driven catalysis. Early examples suggest that NHC-ligated metal complexes anchored on semiconductors can facilitate visible-light-driven CO_2 or water activation. Combining the tunability of NHCs with the light-harvesting capacity of materials like TiO_2, g-C_3N_4, or perovskites could unlock new hybrid photoelectrocatalytic platforms.

Ultimately, a concerted effort that blends real-time spectroscopy, rigorous mechanistic analysis, and the synthetic versatility of NHC chemistry should unlock new frontiers in high-rate, multi-electron electrocatalysis. By addressing the current barriers to ligand cost, nanomaterial scale-up, and MEA integration—while embracing tools like ML and hybrid photoelectrocatalysis—NHC-based platforms may evolve into industrially relevant technologies. Such synergies will be crucial for translating NHC-modified complexes and nanostructures into practical applications—from CO_2-to-fuel converters to next-generation water splitters and nitrogen-cycle electrolysis—that deliver benchmark performance and longevity at scale. By capitalizing on NHC ligands' unique ability to tune metal reactivity across molecular and materials domains, the field is poised to accelerate the development of efficient, durable electrocatalytic systems for sustainable energy applications.

Funding

This research was funded by the Hellenic Foundation for Research and Innovation (H.F.R.I.), Project No. 913 (NANOElectroCAT).

Acknowledgments

A.R. acknowledges support from the Hellenic Foundation for Research and Innovation (H.F.R.I.) under the project NANOElectroCAT (Project No. 913).

Conflicts of Interest

The author declares no conflict of interest.

References

1. Chu, S.; Majumdar, A. Opportunities and Challenges for a Sustainable Energy Future. *Nature* **2012**, *488*, 294–303. https://doi.org/10.1038/nature11475.
2. The Teraton Challenge. A Review of Fixation and Transformation of Carbon Dioxide— Energy & Environmental Science (RSC Publishing) Available online: https://pubs.rsc.org/en/content/articlelanding/2010/ee/b912904a (accessed on 13 July 2025).
3. Firouzjaie, H.A.; Mustain, W.E. Catalytic Advantages, Challenges, and Priorities in Alkaline Membrane Fuel Cells. *ACS Catal.* **2020**, *10*, 225–234. https://doi.org/10.1021/acscatal.9b03892.
4. Ventura-Espinosa, D.; Martín, S.; García, H.; et al. Ligand Effects in the Stabilization of Gold Nanoparticles Anchored on the Surface of Graphene: Implications in Catalysis. *J. Catal.* **2021**, *394*, 113–120. https://doi.org/10.1016/j.jcat.2020.12.027.
5. Shen, Y.; Mu, Y.; Wang, D.; et al. Tuning Electrode Reactivity through Organometallic Complexes. *ACS Appl. Mater. Interfaces* **2023**, *15*, 28851–28878. https://doi.org/10.1021/acsami.3c01726.
6. N-Heterocyclic Carbenes in Late Transition Metal Catalysis | Chemical Reviews. Available online: https://pubs.acs.org/doi/10.1021/cr900074m (accessed on 13 July 2025).
7. Dominique, N.L.; Chandran, A.; Jensen, I.M.; et al. Unmasking the Electrochemical Stability of N-Heterocyclic Carbene Monolayers on Gold. *Chem.-Eur. J.* **2024**, *30*, e202303681. https://doi.org/10.1002/chem.202303681.
8. N-Heterocyclic Carbene Complexes of Copper, Nickel, and Cobalt | Chemical Reviews Available online: https://pubs.acs.org/doi/full/10.1021/acs.chemrev.8b00505?casa_token=5d6H8XuLDFsAAAAA%3A0erF_APQQ41K8fDLDIqwrkXG5F4VgQKgZjsFywvcfo41f2h3JKzGfO7NRuxPIbcjolCtNZgD5RhRoQ (accessed on 13 July 2025).
9. Guo, W.-X.; Shen, Z.-K.; Su, Y.-F.; et al. Iron–N-Heterocyclic Carbene Complexes as Efficient Electrocatalysts for Water Oxidation under Acidic Conditions. *Dalton Trans.* **2022**, *51*, 12494–12501. https://doi.org/10.1039/D2DT01474B.
10. Gao, Y.; Tao, L.; Zhang, Y.-Y.; et al. Enhanced Catalytic Activity of N-Heterocyclic Carbene Stabilized Surface Adatoms for CO Reduction Reaction. *Commun. Chem.* **2023**, *6*, 270. https://doi.org/10.1038/s42004-023-01066-2.
11. Kaeffer, N.; Liu, H.-J.; Lo, H.-K.; et al. An N-Heterocyclic Carbene Ligand Promotes Highly Selective Alkyne Semihydrogenation with Copper Nanoparticles Supported on Passivated Silica. *Chem. Sci.* **2018**, *9*, 5366–5371. https://doi.org/10.1039/C8SC01924J.
12. Rapakousiou, A.; Chalkidis, S.G.; Minadakis, M.P.; et al. NHC–Ni Nanoclusters Covalently Ligated on Carbon Nanotubes: Highly Active Electrocatalysts for the Oxygen Evolution Reaction. *J. Mater. Chem. A* **2025**, *13*, 17489–17498. https://doi.org/10.1039/D5TA00780A.
13. N-Heterocyclic Carbenes as Tunable Ligands for Catalytic Metal Surfaces | Nature Catalysis. Available online: https://www.nature.com/articles/s41929-021-00607-z (accessed on 13 July 2025).
14. Thoi, V.S.; Chang, C.J. Nickel N-Heterocyclic Carbene–Pyridine Complexes That Exhibit Selectivity for Electrocatalytic Reduction of Carbon Dioxide over Water. *Chem. Commun.* **2011**, *47*, 6578–6580. https://doi.org/10.1039/C1CC10449G.
15. Bertini, S.; Rahaman, M.; Dutta, A.; et al. Oxo-Functionalised Mesoionic NHC Nickel Complexes for Selective Electrocatalytic Reduction of CO_2 to Formate. *Green Chem.* **2021**, *23*, 3365–3373. https://doi.org/10.1039/D1GC00388G.
16. Therrien, J.A.; Wolf, M.O.; Patrick, B.O. Electrocatalytic Reduction of CO_2 with Palladium Bis-N-Heterocyclic Carbene Pincer Complexes. *Inorg. Chem.* **2014**, *53*, 12962–12972. https://doi.org/10.1021/ic502056w.
17. Therrien, J.A.; Wolf, M.O.; Patrick, B.O. Polyannulated Bis(N-Heterocyclic Carbene)Palladium Pincer Complexes for Electrocatalytic CO_2 Reduction. *Inorg. Chem.* **2015**, *54*, 11721–11732. https://doi.org/10.1021/acs.inorgchem.5b01698.
18. Agarwal, J.; Shaw, T.W.; Stanton, C.J. III; et al. NHC-Containing Manganese(I) Electrocatalysts for the Two-Electron Reduction of CO2. *Angew. Chem. Int. Ed.* **2014**, *53*, 5152–5155. https://doi.org/10.1002/anie.201311099.
19. Vanden Broeck, S.M.P.; Cazin, C.S.J. Manganese-*N*-Heterocyclic Carbene (NHC) Complexes—An Overview. *Polyhedron* **2021**, *205*, 115204. https://doi.org/10.1016/j.poly.2021.115204.
20. Franco, F.; Pinto, M.F.; Royo, B.; et al. A Highly Active N-Heterocyclic Carbene Manganese(I) Complex for Selective Electrocatalytic CO_2 Reduction to CO. *Angew. Chem. Int. Ed.* **2018**, *57*, 4603–4606. https://doi.org/10.1002/anie.201800705.
21. Richter, M.L.; Peris, E.; Gonell, S. Influence of the Bis-Carbene Ligand on Manganese Catalysts for CO_2 Electroreduction. *ChemSusChem* **2024**, *17*, e202401007. https://doi.org/10.1002/cssc.202401007.
22. Gonell, S.; Assaf, E.A.; Lloret-Fillol, J.; et al. An Iron Bis(Carbene) Catalyst for Low Overpotential CO_2 Electroreduction to CO: Mechanistic Insights from Kinetic Zone Diagrams, Spectroscopy, and Theory. *ACS Catal.* **2021**, *11*, 15212–15222. https://doi.org/10.1021/acscatal.1c04414.
23. An Iron Pyridyl-Carbene Electrocatalyst for Low Overpotential CO_2 Reduction to CO | ACS Catalysis. Available online: https://pubs.acs.org/doi/10.1021/acscatal.0c03798 (accessed on 23 July 2025).
24. Zeng, C.M.; Panetier, J.A. Computational Modeling of Electrocatalysts for CO_2 Reduction: Probing the Role of Primary, Secondary, and Outer Coordination Spheres. *Acc. Chem. Res.* **2025**, *58*, 342–353. https://doi.org/10.1021/acs.accounts.4c00631.

25. Massie, A.A.; Schremmer, C.; Rüter, I.; et al. Selective Electrocatalytic CO_2 Reduction to CO by an NHC-Based Organometallic Heme Analogue. *ACS Catal.* **2021**, *11*, 3257–3267. https://doi.org/10.1021/acscatal.0c04518.
26. Su, X.; McCardle, K.M.; Chen, L.; et al. Robust and Selective Cobalt Catalysts Bearing Redox-Active Bipyridyl-N-Heterocyclic Carbene Frameworks for Electrochemical CO_2 Reduction in Aqueous Solutions. *ACS Catal.* **2019**, *9*, 7398–7408. https://doi.org/10.1021/acscatal.9b00708.
27. Kang, P.; Chen, Z.; Nayak, A.; et al. Catalyst Electrocatalytic Reduction of CO2 in Water to H_2 + CO Syngas Mixtures with Water Oxidation to O_2. *Energy Environ. Sci.* **2014**, *7*, 4007–4012. https://doi.org/10.1039/C4EE01904K.
28. Gonell, S.; Massey, M.D.; Moseley, I.P.; et al. The Trans Effect in Electrocatalytic CO_2 Reduction: Mechanistic Studies of Asymmetric Ruthenium Pyridyl-Carbene Catalysts. *J. Am. Chem. Soc.* **2019**, *141*, 6658–6671. https://doi.org/10.1021/jacs.9b01735.
29. Kearney, L.; Brandon, M.P.; Coleman, A.; et al. Ligand−Structure Effects on N−Heterocyclic Carbene Rhenium Photo− and Electrocatalysts of CO2 Reduction. *Molecules* **2023**, *28*, 4149. https://doi.org/10.3390/molecules28104149.
30. Myren, T.H.T.; Alherz, A.; Stinson, T.A.; et al. Metalloradical Intermediates in Electrocatalytic Reduction of CO_2 to CO: Mn versus Re Bis-N-Heterocyclic Carbene Pincers. *Dalton Trans.* **2020**, *49*, 2053–2057. https://doi.org/10.1039/C9DT04691G.
31. Friães, S.; Realista, S.; Mourão, H.; et al. N-Heterocyclic and Mesoionic Carbenes of Manganese and Rhenium in Catalysis. *Eur. J. Inorg. Chem.* **2022**, *2022*, e202100884. https://doi.org/10.1002/ejic.202100884.
32. Huang, C.; Liu, J.; Huang, H.-H.; et al. Recent Progress in Electro- and Photo-Catalytic CO_2 Reduction Using *N*-Heterocyclic Carbene Transition Metal Complexes. *Polyhedron* **2021**, *203*, 115147. https://doi.org/10.1016/j.poly.2021.115147.
33. Cao, Z.; Kim, D.; Hong, D.; et al. A Molecular Surface Functionalization Approach to Tuning Nanoparticle Electrocatalysts for Carbon Dioxide Reduction. *J. Am. Chem. Soc.* **2016**, *138*, 8120–8125. https://doi.org/10.1021/jacs.6b02878.
34. Vickers, J.W.; Alfonso, D.; Kauffman, D.R. Electrochemical Carbon Dioxide Reduction at Nanostructured Gold, Copper, and Alloy Materials. *Energy Technol.* **2017**, *5*, 775–795. https://doi.org/10.1002/ente.201600580.
35. Cao, Z.; Derrick, J.S.; Xu, J.; et al. Chelating N-Heterocyclic Carbene Ligands Enable Tuning of Electrocatalytic CO_2 Reduction to Formate and Carbon Monoxide: Surface Organometallic Chemistry. *Angew. Chem. Int. Ed.* **2018**, *57*, 4981–4985. https://doi.org/10.1002/anie.201800367.
36. Luo, Q.; Duan, H.; McLaughlin, M.C.; et al. Why Surface Hydrophobicity Promotes CO_2 Electroreduction: A Case Study of Hydrophobic Polymer N-Heterocyclic Carbenes. *Chem. Sci.* **2023**, *14*, 9664–9677. https://doi.org/10.1039/D3SC02658B.
37. Chen, Y.; Wei, K.; Duan, H.; et al. N-Heterocyclic Carbene Polymer-Stabilized Au Nanowires for Selective and Stable Reduction of CO_2. *J. Am. Chem. Soc.* **2025**, *147*, 14845–14855. https://doi.org/10.1021/jacs.5c04742.
38. Kolding, K.N.; Bretlau, M.; Zhao, S.; et al. NHC-CDI Ligands Boost Multicarbon Production in Electrocatalytic CO_2 Reduction by Increasing Accumulated Charged Intermediates and Promoting *CO Dimerization on Cu. *J. Am. Chem. Soc.* **2024**, *146*, 13034–13045. https://doi.org/10.1021/jacs.3c14306.
39. Narouz, M.R.; Osten, K.M.; Unsworth, P.J.; et al. N-Heterocyclic Carbene-Functionalized Magic-Number Gold Nanoclusters. *Nat. Chem.* **2019**, *11*, 419–425. https://doi.org/10.1038/s41557-019-0246-5.
40. Chen, Z.; Zuo, D.; Zhao, L.; et al. Electrochemical Dechlorination Promotes Syngas Production in N-Heterocyclic Carbene Protected Au_{13} Nanoclusters. *Chem. Sci.* **2025**, *16*, 10397–10413. https://doi.org/10.1039/D5SC00896D.
41. Kulkarni, V.K.; Khiarak, B.N.; Takano, S.; et al. N-Heterocyclic Carbene-Stabilized Hydrido Au24 Nanoclusters: Synthesis, Structure, and Electrocatalytic Reduction of CO_2. *J. Am. Chem. Soc.* **2022**, *144*, 9000–9006. https://doi.org/10.1021/jacs.2c00789.
42. Levchenko, T.I.; Yi, H.; Aloisio, M.D.; et al. Electrocatalytic CO_2 Reduction with Atomically Precise Au_{13} Nanoclusters: Effect of Ligand Shell on Catalytic Performance. *ACS Catal.* **2024**, *14*, 4155–4163. https://doi.org/10.1021/acscatal.3c06114.
43. Tappan, B.A.; Chen, K.; Lu, H.; Sharada, S.M.; Brutchey, R.L. Synthesis and Electrocatalytic HER Studies of Carbene-Ligated $Cu_{3-x}P$ Nanocrystals. *ACS Appl. Mater. Interfaces* **2020**, *12*, 16394–16401. https://doi.org/10.1021/acsami.0c00025.
44. Brinda, K.N.; Małecki, J.G.; Yhobu, Z.; et al. Novel Carbene Anchored Molecular Catalysts for Hydrogen Evolution Reactions. *J. Phys. Chem. C* **2021**, *125*, 3793–3803. https://doi.org/10.1021/acs.jpcc.0c06701.
45. Markandeya, G.B.; Yhobu, Z.; Małecki, J.G.; et al. Palladium(II)–N-Heterocyclic Carbene Complex-Based Electrocatalysts for Hydrogen Evolution Reaction. *Energy Fuels* **2023**, *37*, 2237–2244. https://doi.org/10.1021/acs.energyfuels.2c04124.
46. Brinda, K.N.; Yhobu, Z.; Małecki, J.G.; et al. Novel Coumarin Substituted N–Heterocyclic Carbene Ag(I), Au(I) and Ni(II) Complexes as Electrocatalysts in Hydrogen Evolution Reactions from Water. *Int. J. Hydrogen Energy* **2023**, *48*, 10911–10921. https://doi.org/10.1016/j.ijhydene.2022.12.124.
47. Shahadat, H.M.; Ahmad, N.; Khattak, Z.A.K.; et al. Highly Active Macrocyclic Nickel(II) Complex for Hydrogen Evolution Reaction in Neutral Aqueous Conditions. *Int. J. Hydrogen Energy* **2023**, *48*, 33927–33936. https://doi.org/10.1016/j.ijhydene.2023.05.192.
48. Vijayakumar, M.; Małecki, J.G.; Nagaraju, D.H.; et al. Impact of Ligand Modification on the Hydrogen Evolution Reaction of Highly Active Silver(I)- and Ruthenium(II)-N-Heterocyclic Carbene-Based Electrocatalysts: Comprehension from the Hydrogen Oxidation Reaction. *ACS Appl. Energy Mater.* **2024**, *7*, 4813–4825. https://doi.org/10.1021/acsaem.4c00523.

49. Yhobu, Z.; Markandeya, G.B.; Małecki, J.G.; et al. Enhancing Electrochemical Hydrogen Evolution Performance of N-Heterocyclic Carbene-Coordinated Palladium(II) Complexes with Conductive Carbon: Insights from Hydrogen Oxidation Reactions. *ACS Appl. Energy Mater.* **2024**, *7*, 1202–1211. https://doi.org/10.1021/acsaem.3c02779.
50. Si, S.; Song, W.; Chen, J.; et al. Neutral Nickel Complexes with Tetradentate N-Heterocyclic Carbene Amidate Ligands for Electrocatalytic Hydrogen Evolution. *Dalton Trans.* **2024**, *53*, 19088–19092. https://doi.org/10.1039/D4DT02746A.
51. Yhobu, Z.; Patel, M.J.; Małecki, J.G.; et al. Mono- vs. Tri-Nuclear Silver(I) and Gold(I) N-Heterocyclic Carbene Complexes/Metallacycles as Free-Standing Carbon Cloth Electrodes for Hydrogen Evolution Reaction in Alkaline Medium. *Energy Fuels* **2024**, *38*, 23058–23067. https://doi.org/10.1021/acs.energyfuels.4c04103.
52. Mandal, S.K.; Sunil, C.; Choudhury, J. [Fe]-Hydrogenase-Inspired Proton-Shuttle Installation in a Molecular Cobalt Complex for High-Efficiency H_2 Evolution Reaction. *ACS Catal.* **2024**, *14*, 2058–2070. https://doi.org/10.1021/acscatal.3c04879.
53. Rapakousiou, A.; Minadakis, M.P.; Chalkidis, S.G.; et al. Nanoarchitectured N-Heterocyclic Carbene-Pt Nanoparticles on Carbon Nanotubes: Toward Advanced Electrocatalysis in the Hydrogen Evolution Reaction. *ACS Appl. Mater. Interfaces* **2025**, *17*, 28138–28150. https://doi.org/10.1021/acsami.5c02182.
54. Shahadat, H.M.; Younus, H.A.; Ahmad, Net al. Homogenous Electrochemical Water Oxidation by a Nickel(II) Complex Based on a Macrocyclic N-Heterocyclic Carbene/Pyridine Hybrid Ligand. *Catal. Sci. Technol.* **2019**, *9*, 5651–5659. https://doi.org/10.1039/C9CY01485C.
55. Sánchez-Page, B.; Pérez-Mas, A.M.; González-Ingelmo, M.; et al. Influence of Graphene Sheet Properties as Supports of Iridium-Based N-Heterocyclic Carbene Hybrid Materials for Water Oxidation Electrocatalysis. *J. Organomet. Chem.* **2020**, *919*, 121334. https://doi.org/10.1016/j.jorganchem.2020.121334.
56. González-Ingelmo, M.; Álvarez, P.; Granda, M.; et al. On the Study of the Preparation of Graphene-Anchored NHC-Iridium Catalysts from a Coke-like Waste with Application in Water Splitting. *Appl. Surf. Sci.* **2024**, *655*, 159556. https://doi.org/10.1016/j.apsusc.2024.159556.
57. Yhobu, Z.; Markandeya, G.B.; Małecki, J.G.; et al. Pyridine-Functionalized N-Heterocyclic Carbene Gold(I) Binuclear Complexes as Molecular Electrocatalysts for Oxygen Evolution Reactions. *Appl. Organomet. Chem.* **2022**, *36*, e6837. https://doi.org/10.1002/aoc.6837.
58. Vijayakumar, M.; Yhobu, Z.; Małecki, J.G.; et al. Comprehensive Enhancement in Electrocatalytic Oxygen Evolution Performance of Nickel and Cobalt Complexes Derived from π-Conjugated N-Heterocyclic Carbene Ligands through Carbon Composite Strategy. *Catal. Sci. Technol.* **2024**, *14*, 2489–2502. https://doi.org/10.1039/D3CY01732J.
59. Sampatkumar, H.G.; Patra, A.; Antony, A.M.; et al. A Sustainable Anchoring of Palladium Nanoparticles on Waste Plastic Derived Functionalized Robust Carbon: There of Application in Sensing of Genotoxic Bio-Thiol Compound and Oxygen Evolution Activity. *Chem. Eng. Sci.* **2025**, *307*, 121334. https://doi.org/10.1016/j.ces.2025.121334.
60. Yhobu, Z.; Patel, M.J.; Małecki, J.G.; et al. Non-Covalent Immobilization of Metal N-Heterocyclic Carbene Complexes onto Carbon Cloth as Bifunctional Electrodes for Overall Water Splitting in Alkaline Medium. *ACS Appl. Energy Mater.* **2024**, *7*, 9500–9511. https://doi.org/10.1021/acsaem.4c02127.
61. Vijayakumar, M.; Achar, G.; Yhobu, Z.; et al. Augmenting the Electrocatalytic Activities of Metal–N-Heterocyclic Carbene Complexes as Bifunctional Electrocatalysts for Hydrogen and Oxygen Evolution Reactions by Carbon Composite Strategy. *Energy Fuels* **2024**, *38*, 5421–5432. https://doi.org/10.1021/acs.energyfuels.3c04793.
62. Daniel, S.; Vijayakumar, M.; Gandigawad, A.; et al. Nickel(II)–N-Heterocyclic Carbene Complex and Its Carbon Nanotube Composites as Efficient Bifunctional Electrocatalysts for Hydrogen and Oxygen Evolution Reactions and Mercury-Sensing Applications. *Energy Fuels* **2024**, *38*, 14632–14644. https://doi.org/10.1021/acs.energyfuels.4c01848.
63. Liu, L.; Johnson, S.I.; Appel, A.M.; et al. Oxidation of Ammonia Catalyzed by a Molecular Iron Complex: Translating Chemical Catalysis to Mediated Electrocatalysis. *Angew. Chem. Int. Ed.* **2024**, *63*, e202402635. https://doi.org/10.1002/anie.202402635.
64. Zhang, J.; Zhang, Y.; Qin, Z.; et al. How Carbene Ligands Transform AuAg Alloy Nanoclusters for Electrocatalytic Urea Synthesis. *Angew. Chem. Int. Ed.* **2025**, *64*, e202420993. https://doi.org/10.1002/anie.202420993.
65. Su, X.; McCardle, K.M.; Panetier, J.A.; et al. Electrocatalytic CO_2 Reduction with Nickel Complexes Supported by Tunable Bipyridyl-N-Heterocyclic Carbene Donors: Understanding Redox-Active Macrocycles. *Chem. Commun.* **2018**, *54*, 3351–3354. https://doi.org/10.1039/C8CC00266E.
66. Weder, N.; Probst, B.; Sévery, L.; et al. Mechanistic Insights into Photocatalysis and over Two Days of Stable H2 Generation in Electrocatalysis by a Molecular Cobalt Catalyst Immobilized on TiO_2. *Catal. Sci. Technol.* **2020**, *10*, 2549–2560. https://doi.org/10.1039/D0CY00330A.